DECEMBER 2012

SAN FRANCISCO ESTUARY & WATERSHED SCIENCE
Sponsored by the Delta Science Program and the UC Davis John Muir Institute of the Environment

# Downscaling Future Climate Projections to the Watershed Scale: a North San Francisco Bay Estuary Case Study

**Elisabeth Micheli[1†], Lorraine Flint[2], Alan Flint[2], Stuart Weiss[3], and Morgan Kennedy[1]**

## ABSTRACT

We modeled the hydrology of basins draining into the northern portion of the San Francisco Bay Estuary (North San Pablo Bay) using a regional water balance model (Basin Characterization Model; BCM) to estimate potential effects of climate change at the watershed scale. The BCM calculates water balance components, including runoff, recharge, evapotranspiration, soil moisture, and stream flow, based on climate, topography, soils and underlying geology, and the solar-driven energy balance. We downscaled historical and projected precipitation and air temperature values derived from weather stations and global General Circulation Models (GCMs) to a spatial scale of 270 m. We then used the BCM to estimate hydrologic response to climate change for four scenarios spanning this century (2000–2100). Historical climate patterns show that Marin's coastal regions are typically on the order of 2 °C cooler and receive five percent more precipitation compared to the inland valleys of Sonoma and Napa because of marine influences and local topography. By the last 30 years of this century, North Bay scenarios project average minimum temperatures to increase by 1.0 °C to 3.1 °C and average maximum temperatures to increase by 2.1 °C to 3.4 °C (in comparison to conditions experienced over the last 30 years, 1981–2010). Precipitation projections for the 21st century vary between GCMs (ranging from 2 to 15% wetter than the 20th-century average). Temperature forcing increases the variability of modeled runoff, recharge, and stream discharge, and shifts hydrologic cycle timing. For both high- and low-rainfall scenarios, by the close of this century warming is projected to amplify late-season climatic water deficit (a measure of drought stress on soils) by 8% to 21%. Hydrologic variability within a single river basin demonstrated at the scale of subwatersheds may prove an important consideration for water managers in the face of climate change. Our results suggest that in arid environments characterized by high topo-climatic variability, land and water managers need indicators of local watershed hydrology response to complement regional temperature and precipitation estimates. Our results also suggest that temperature forcing may generate greater drought stress affecting soils and stream flows than can be estimated by variability in precipitation alone.

† Corresponding author: *lmicheli@pepperwoodpreserve.org*
1 Dwight Center for Conservation Science at Pepperwood, Santa Rosa, CA 95404
2 U.S. Geological Survey, Sacramento, CA 95819
3 Creekside Center for Earth Observation, Menlo Park, CA 94025

## KEY WORDS

Climate change, watershed hydrology, downscaling, San Pablo Bay, Basin Characterization Model, stream flow, aquifer recharge, climatic water deficit.

## INTRODUCTION

Competently adapting to climate change requires watershed planning based on the best estimates science can provide of potential changes to local climate and the hydrologic cycle that supports our water resources and other valuable ecosystem services. Application of projected climate data to evaluate effects at the watershed scale requires downscaling from the 2.5° spatial scale (approximately 250 km) of current General Circulation Model (GCM) outputs. Downscaling entails the calculation of fine-scale information on the basis of coarser-scale information using various methods of statistical and spatial interpolation. New approaches to downscale GCM projections to finer spatial scales can reproduce empirically validated results for air temperature and precipitation, providing the opportunity to apply physically based models that are grounded in local watershed data to assess future climate effects at meaningful hydrological and ecological scales (Flint and Flint 2012a). The purpose of downscaling to the watershed scale is to create planning scenarios that adequately capture local variability in climate and hydrology. Understanding this variability may hold the key to helping managers identify zones of both watershed vulnerability and resilience in the face of climate change.

Applying these results effectively requires understanding limits to localized estimates of potential climate change. Watershed-scale climate and hydrology projections illustrate a range of planning scenarios capable of describing patterns and variability of historic climate data. Models can estimate ranges of natural variability, project directions and the magnitude of decade-to-century trends, and quantify model uncertainty. Modeled scenarios are not intended to predict shorter-term changes in weather, but instead to project long-term climate trends, based on a range of scenarios that provide realistic depictions of potential hydrology outcomes that result from a warming climate. For effective adaptive management, real-time field data collection of watershed indicators will be crucial to test hypotheses illustrated here against future climate scenarios.

## SETTING

San Francisco's North Bay region (Figure 1) is a complex mosaic of land forms, vegetation types, land uses, and climate influences that range from coastal to inland conditions (BAOSC 2011). The jurisdiction of the North Bay Watershed Association (NBWA), the core of our study area, comprises approximately 2,200 km$^2$, which includes 25% of the watershed area that drains directly into the San Francisco Bay estuary. Nearly a half-million people live in the North Bay, less than 8% of the population of the entire bay area (NBWA 2003). At the southern limit of California's North Coast range, the region is tectonically active and typified by varied topography comprised of low mountain ranges that frame north–south trending alluvial valleys. The majority of watersheds examined here drain directly to the San Francisco Bay (except for coastal Marin County, which drains directly to the Pacific Ocean and lies outside of NBWA's jurisdiction), and thus transition from rugged montane headwaters to depositional estuarine environments. Ecologically the bay area is considered a global "hotspot" of biodiversity, as biological diversity exploits the myriad of habitat types generated by the climatic and geomorphic diversity of the region (Loarie and others 2009).

The major basins defined for this study form a west–east transect across the North Bay and include; "Marin Coast" (coastal drainages ranging from the Marin Headlands to Point Reyes), "Marin Bay" (Marin drainages discharging to the Bay), Petaluma River watershed, Sonoma Creek watershed, and the Napa River watershed (Figure 1). Excluding the Marin Coast basin, the core of the study area comprises the geographic jurisdiction of the NBWA. These major planning basins can be further divided into minor basins according to watershed delineations generated by the Natural Resources Conservation Service's California Interagency Watershed Mapping Committee (CalWater 1999, see Appendix A). Marin

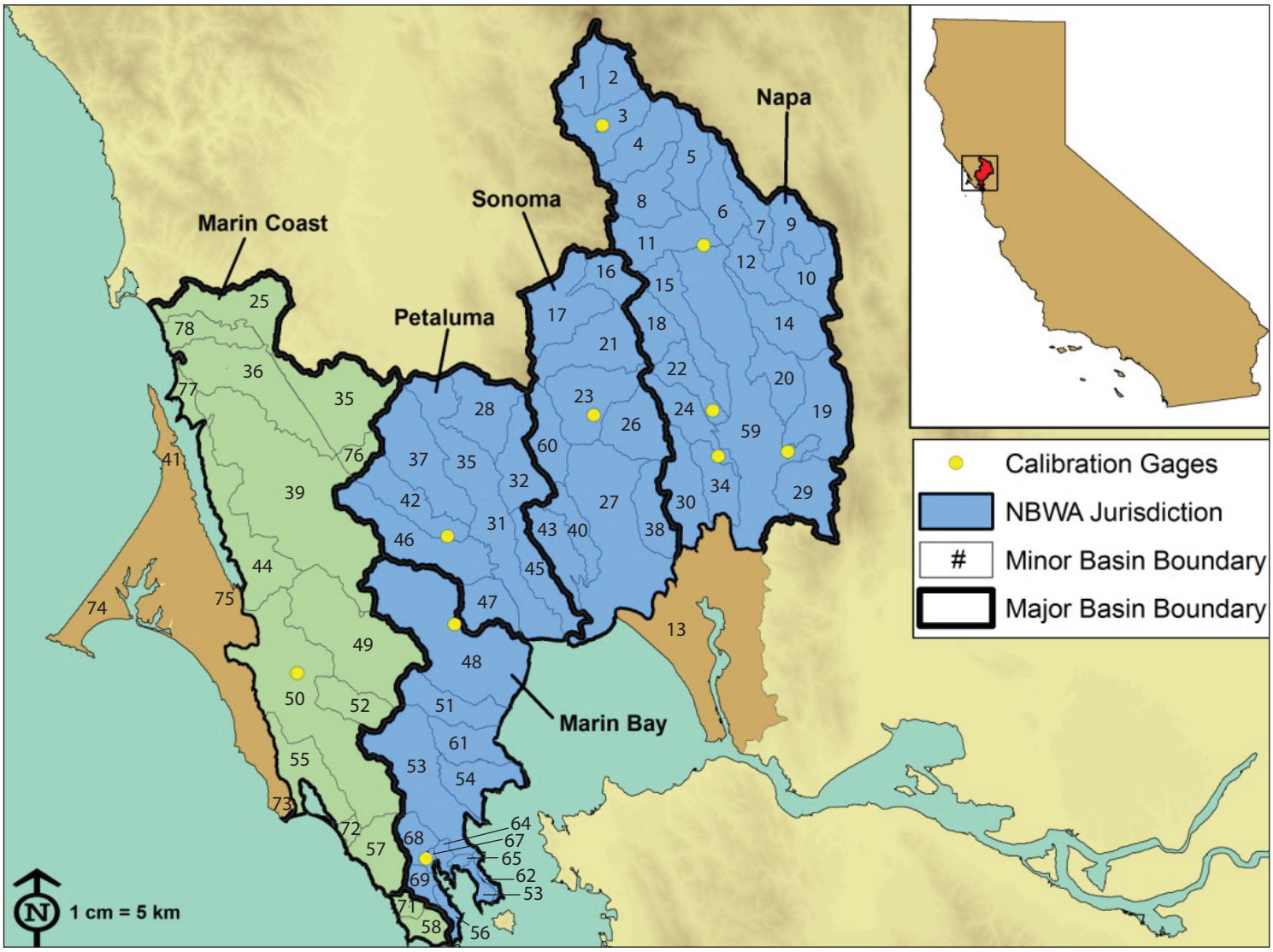


**Figure 1** Study area of major and minor basins analyzed using the BCM. Blue areas define NBWA jurisdiction, which we term "North Bay region." Numbers label minor basins (see Appendix A). Table 1 describes calibration gages (yellow circles) used for the BCM.

**Table 1** USGS stream calibration gages used for the BCM

| USGS stream calibration gage | USGS# | Period of record | Ratio of measured to modeled runoff |
|---|---|---|---|
| Napa River near St. Helena | 11456000 | 1975–1983 | 0.983 |
| Novato Creek at Novato | 11459500 | 1960–1990 | 0.990 |
| Sonoma Creek at Agua Caliente | 11458500 | 1960–1980 | 0.994 |
| San Antonio Creek near Petaluma | 11459300 | 1975–1981 | 1.007 |
| Milliken Creek near Napa | 11458100 | 1970–1983 | 1.009 |
| Dry Creek near Napa | 11457000 | 1959–1966 | 0.988 |
| Napa River at Calistoga | 11455900 | 1975–1982 | 0.996 |
| Arroyo Corte Madera at Mill Valley | 11460100 | 1965–1985 | 1.009 |

is the most densely populated area, and is geologically distinguished by impermeable bedrock basins and limited aquifer recharge. Petaluma, Sonoma, and Napa support both urban and agricultural development, including rural residential communities that dwell at the urban–wildland interface. North Bay communities rely on a varied portfolio of water sources—imported water (generally from sources further north) conveyed via aqueduct, surface storage, and, where applicable, groundwater basins, where there is an emerging emphasis on conjunctive use of surface–groundwater supplies. Unlike the majority of California, snowmelt is not a significant component of the water cycle for the North Bay, although it may impact available imports.

Historic climate data for the North Bay reveals high spatial and temporal variability, which adds to uncertainties associated with climate projections. In the context of global climate projections, the region is located in a transition zone between warmer and wetter winters projected for Oregon and Washington, and warmer and drier conditions projected for the south of California and Baja Mexico (Knowles and Cayan 2002; Cayan and others 2008, 2009). While average precipitation is, therefore, not consistently projected to shift towards a specifically wetter or drier climate, we selected GCM scenarios that project both more and, ultimately, less precipitation, compared to historic conditions. Study results thus illustrate how projected increases in air temperatures for North Bay watersheds may impact the hydrologic cycle, particularly the relative ratios of evapotranspiration, runoff, and recharge, for both "wetter" and "drier" future scenarios.

## METHODS

### Basin Characterization Model

Watershed hydrology of North Bay drainages is the result of interactions among precipitation, surface water runoff, and infiltration (including direct recharge or groundwater interaction with streams, rivers, and lakes). Runoff, recharge, and changes in soil moisture conditions can be estimated using a simple monthly water balance approach. The Basin Characterization Model (BCM) is a physically based model that calculates water balance fractions based on data inputs for topography, soil composition and depth, underlying bedrock geology, and spatially distributed values (measured or estimated) of air temperature and precipitation (Flint and Flint 2007, 2012a).

The BCM calculates monthly recharge and runoff using a deterministic water-balance approach based on the distribution of precipitation and the estimation of potential evapotranspiration (Flint and Flint 2007, 2012a). The BCM relies on a rigorous hourly energy balance calculation that uses topographic shading and applies available spatial maps of elevation, bedrock permeability estimated from geology, soil water storage from Soil Survey Geographic (SSURGO) soil databases (NRCS 2006), and the empirically based Parameter-Elevation Regressions on Independent Slopes Model (PRISM) precipitation and air temperature database and maps (Daly and others 2004). The BCM can be used to identify locations and climatic conditions that generate excess water by quantifying the amount of water available either as runoff or as in-place recharge on a monthly basis.

The BCM is calibrated regionally to measure potential evapotranspiration data and Moderate Resolution Imaging Spectroradiometer (MODIS) snow cover data (Flint and Flint 2007). Locally, the model is also calibrated to measured unimpaired streamflow data. The determination of whether excess water becomes recharge or runoff is governed in part by the underlying bedrock permeability. The higher the bedrock permeability, the higher the recharge and the lower the runoff generated for a given grid cell. In small gaged basins that generate unimpaired flows, the bedrock permeability can be adjusted to calculate a total basin discharge that matches the measured basin discharge as shown in Figure 2. In the North Bay, eight stream gages shown in Figure 1 were used to calibrate the model. These gages are listed in Table 1 with their location description, USGS numerical identifier, and the ratio of measured data to modeled data for each period of record.

Temperature and precipitation are two primary drivers of physical processes acting at the watershed scale. BCM hydrologic variables sensitive to temperature include potential evapotranspiration (PET)

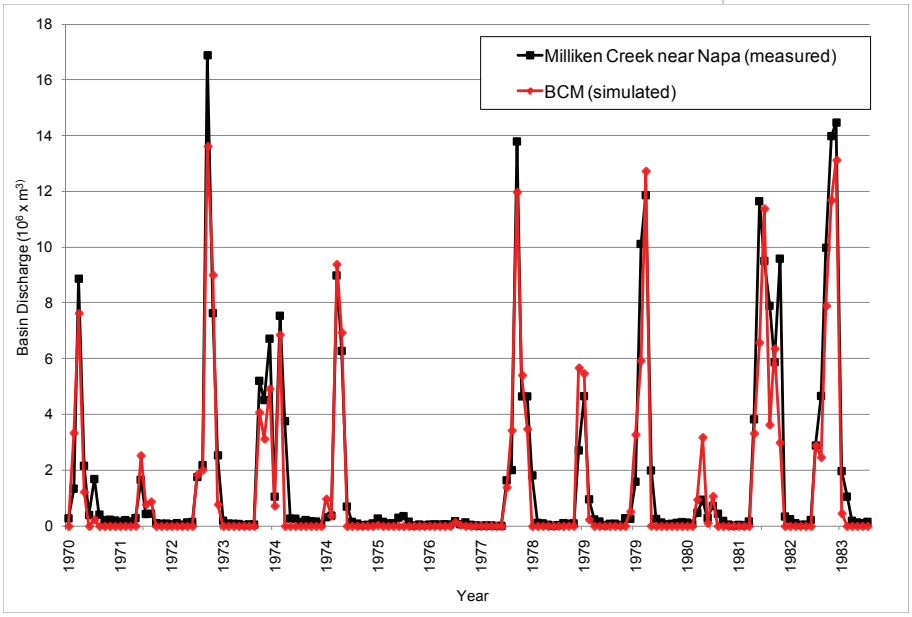


**Figure 2** Model calibration example: comparison of modeled and measured monthly stream discharge, Milliken Creek, Napa River basin, 1970–1983. Monthly stream discharge measured at USGS gage #11458100 (Milliken Creek near Napa) in black (square labels) compared to Basin Characterization Model (BCM) stream discharge measurements in red (diamond labels) produced via calibration run. Each gage shown in Figure 1 was used for model calibration to ensure the BCM effectively captures magnitude and timing of peaks in monthly discharge.

and actual evapotranspiration (AET). BCM variables sensitive to quantities of precipitation include runoff and recharge. Climatic water deficit (CWD), defined in more detail below, combines the effects of precipitation inputs and temperature forcing by tracking soil moisture changes over time.

## Characterizing Historic Patterns of Climate Variability

Historical values for monthly averaged precipitation and air temperature are available in a gridded map format at a 4-km spatial scale from PRISM for the North Bay study area from 1896 through 2009 (Daly and others 2004). We spatially downscaled the coarse-resolution grids (4 km) to produce fine-resolution grids (270 m) on the basis of a model developed by Nalder and Wein (1998).

Our technique combines a spatial Gradient and Inverse Distance Squared (GIDS) weighting to monthly point or grid data using multiple regressions calculated for every grid cell for every month. Using the 4-km-resolution digital elevation model in PRISM, parameter weighting is based on the location and elevation of the new fine-resolution grid relative to existing coarse-resolution grid cells (Flint and Flint 2012a). To remove the "bullseye" effect often associated with certain interpolation schemes (i.e., kriging, inverse distance squared, etc.), we modified the program to have a search radius that is specified as the size of grid cell of the coarse-resolution grid. The modified GIDS spatial downscaling technique does not introduce additional uncertainty in the downscaling process, and may indeed improve the estimate of the climate variable by incorporating the deterministic influence (such as lapse rates or rain shadows) of location and elevation on climate. The details of the methodology and the evaluation of uncertainty are discussed in Flint and Flint (2012a).

To illustrate fine-scale geographic patterns of historic climate change over the last century, we applied a regression to the downscaled PRISM data for annual averages for every 270-m grid cell to calculate the magnitude and direction of observed changes in precipitation and air temperature for decadal time intervals over the last century (Table 2).

## Downscaling Future Climate Scenarios

Global future climate scenarios created through the application of GCMs and distributed by the Intergovernmental Panel on Climate Change (IPCC) estimate future spatial patterns of temperature and precipitation in response to greenhouse gas forcing at a global scale. GCMs are generally available for the continental U.S. at 12-km spatial resolution

**Table 2** Monthly measured climate and simulated hydrologic parameters for 1901–2010 averaged by decade

| Model | Time Interval | Maximum air temperature | | Minimum air temperature | | Precipitation | | Runoff | | Recharge | | Potential evapo-transpiration | | Climatic water deficit | |
|---|---|---|---|---|---|---|---|---|---|---|---|---|---|---|---|
| | | °C | SE | °C | SE | mm $y^{-1}$ | SE | mm $y^{-1}$ | SE | mm $y^{-1}$ | SE | mm $y^{-1}$ | SE | mm $y^{-1}$ | SE |
| Historic[a] | 1921–50 | 21.1 | 0.1 | 6.4 | 0.1 | 740 | 43 | 184 | 22 | 85 | 8 | 1,170 | 4 | 696 | 17 |
| | 1951–80 | 21.3 | 0.1 | 7.0 | 0.1 | 816 | 48 | 236 | 26 | 98 | 9 | 1,181 | 4 | 695 | 17 |
| | 1981–10 | 21.7 | 0.1 | 7.9 | 0.1 | 874 | 59 | 269 | 32 | 107 | 11 | 1,212 | 4 | 707 | 20 |
| GFDL A2[b] | 2011–40 | 22.6 | 0.1 | 8.4 | 0.1 | 864 | 56 | 236 | 27 | 117 | 12 | 1,226 | 3 | 710 | 20 |
| | 2041–70 | 23.2 | 0.1 | 9.1 | 0.1 | 860 | 68 | 266 | 38 | 122 | 16 | 1,242 | 3 | 766 | 17 |
| | 2071–00 | 25.1 | 0.1 | 11.0 | 0.1 | 699 | 54 | 187 | 27 | 89 | 10 | 1,286 | 3 | 855 | 19 |
| GFDL B1[b] | 2011–40 | 22.7 | 0.1 | 8.6 | 0.7 | 913 | 84 | 308 | 49 | 132 | 18 | 1,228 | 3 | 750 | 19 |
| | 2041–70 | 23.4 | 0.1 | 9.2 | 0.5 | 858 | 56 | 243 | 32 | 118 | 12 | 1,244 | 2 | 742 | 15 |
| | 2071–00 | 23.9 | 0.1 | 9.6 | 0.5 | 729 | 52 | 189 | 28 | 86 | 11 | 1,253 | 2 | 792 | 16 |
| PCM A2[b] | 2011–40 | 22.7 | 0.1 | 7.9 | 0.5 | 882 | 67 | 250 | 37 | 121 | 14 | 1,221 | 2 | 706 | 19 |
| | 2041–70 | 23.7 | 0.1 | 8.9 | 0.5 | 882 | 58 | 266 | 36 | 119 | 13 | 1,243 | 2 | 740 | 15 |
| | 2071–00 | 24.8 | 0.1 | 10.0 | 0.5 | 943 | 82 | 313 | 50 | 131 | 17 | 1,268 | 2 | 758 | 21 |
| PCM B1[b] | 2011–40 | 22.7 | 0.1 | 7.9 | 0.6 | 1,051 | 78 | 369 | 45 | 160 | 18 | 1,220 | 2 | 692 | 19 |
| | 2041–70 | 23.1 | 0.1 | 8.3 | 0.5 | 913 | 77 | 284 | 47 | 121 | 16 | 1,229 | 2 | 717 | 20 |
| | 2071–00 | 23.8 | 0.1 | 8.9 | 0.5 | 907 | 65 | 281 | 39 | 120 | 13 | 1,243 | 2 | 732 | 18 |

a Derived from PRISM climate data (Daly and others 2004)
b Derived from GCM climate projections (IPCC2001). Hydrologic variables are simulated from the Basin Characterization Model.

(IPCC 2001, 2007). A set of these projections have been downscaled to 12 km for the State of California and its environs by researchers at USGS and Scripps Institute of Oceanography using the constructed analogs method of Hidalgo and others (2008). These statistically downscaled projections provide a basis for our further spatial downscaling for model application.

Our goal was to represent climate projections for California on the basis of GCMs that have proven capable of simulating recent historical climate, particularly the distribution of monthly temperatures and the strong seasonal cycle of precipitation that exists in the region (Knowles and Cayan 2002; Cayan and others 2008, 2009). In addition, models were selected to represent a range of model sensitivity to greenhouse gas forcing. On the basis of these criteria, we selected two GCMs: the Parallel Climate Model (PCM) developed by National Center for Atmospheric Research (NCAR) and Department of Energy (DOE) (see Washington and others 2000; Meehl and others 2003) and the National Oceanic and Atmospheric Administration (NOAA) Geophysical Fluid Dynamics Laboratory CM2.1 model (GFDL) (Delworth and others 2006; Stouffer and others 2006). The choice of greenhouse gas emissions scenarios—A2 (medium-high, essentially "business as usual") and B1 (low, essentially a "mitigated emissions" scenario)—was guided by considerations presented by the IPCC (Nakic´enovic´ and others 2000). Thus, we developed a range of hydrology estimates based on four specific scenarios: two models each representing two emissions scenarios. We refer to these scenarios as "GFDL A2," "GFDL B1," "PCM A2," and "PCM B1." For reasons described in detail below, we generalize GFDL scenarios as "warmer–drier" and PCM scenarios as "warmer–wetter."

These four scenarios were spatially downscaled from the 12-km grid scale to the historical PRISM data scale of 4 km to correct bias. To make the correction possible, the GCM is run for a historical forcing function to establish a baseline for modeling to match current climate. The baseline period for this study is

defined as the PCM and GFDL model runs for 1950–2000, when climate change forcings are assumed absent from the model, representing current (pre–2000) atmospheric greenhouse gas conditions. This baseline period was then adjusted using the PRISM data from 1950–2000, for each month and for each grid cell. Our approach to bias correction is a simple scaling of the mean and standard deviation of the projections to match those of the PRISM data, following Bouwer and others (2004) and described in detail in Flint and Flint (2012a). Once the bias correction is complete, the 4-km projections are further downscaled to 270-m spatial resolution using the GIDS spatial interpolation approach for model application.

### Climatic Water Deficit

The term "climatic water deficit" defined by Stephenson (1998; Figure 3), is quantified as the amount of water by which PET exceeds AET. This term effectively integrates the combined effects of solar radiation, evapotranspiration, and air temperature on watershed conditions, given available soil moisture derived from precipitation. Climatic water deficit can be thought of as the amount of additional water that would have evaporated or transpired had it been present in the soils, given the temperature-forcing. This calculation is an estimate of drought stress on soils and plants, and recent studies suggest it may serve as an effective control on vegetation cover types in the Bay Area (Cornwell and others 2012). In a Mediterranean climate, CWD can also be thought of as a surrogate for water demand based on irrigation needs, and changes in CWD effectively quantify the supplemental amount of water needed to maintain current vegetation cover, whether natural vegetation or agricultural crops.

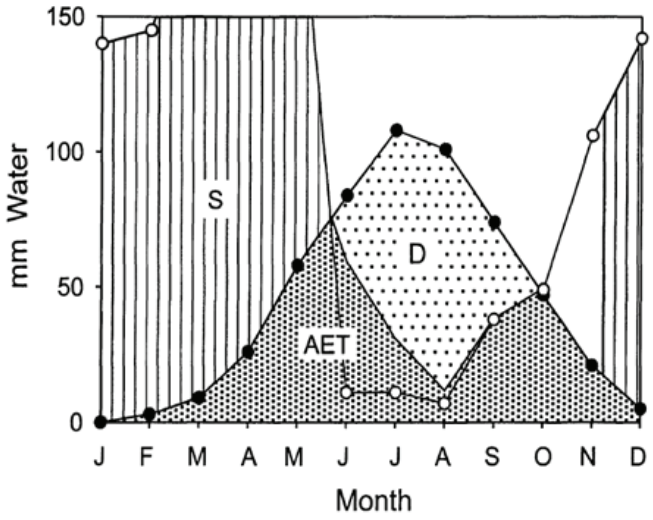


**Figure 3** Climatic water deficit quantifies evaporative demand that exceeds available soil moisture, where S = soil moisture, AET = actual evapotranspiration, and D = climatic water deficit. Source: Stephenson (1998).

### Basin Characterization Model Data Analysis

The BCM estimates 16 hydrologic parameters at monthly time intervals for approximately 2 centuries over a set of grid points spaced 270 m apart (Flint and Flint 2012b). For the North Bay study area (approximately 2,820 km$^2$, NBWA jurisdiction plus Marin Coast major basin, Figure 1), this amounts to a data set comprising approximately 38,680 monthly parameters that span historic (1896–2000) and projected (2000–2100) time periods for four scenarios. Data was aggregated at the scales of CalWater minor basins, major planning basins, and the region as a whole (Appendices A and B). In analyzing and visually representing the data, we calculated average annual values for decades and 30-year time intervals to document long-term trends rather than displaying the details of variable inter-annual conditions. Maps of spatial distributions of parameters were made using sub-basins as the smallest unit of analysis, rather than displaying values at the scale of the 270-m grid (Figure 4A–F).

## RESULTS

### Historic Climate Variability

Analysis of historic PRISM data demonstrates that climate change in the North Bay is well underway, yet patterns of change are highly variable spatially. Table 2 provides a summary of historical monthly values for key parameters averaged over decadal intervals. Average maximum temperatures have increased from 20.3 °C (1901–1910) to 21.7 °C (1991–2000), amounting to a net increase of 1.4 °C and

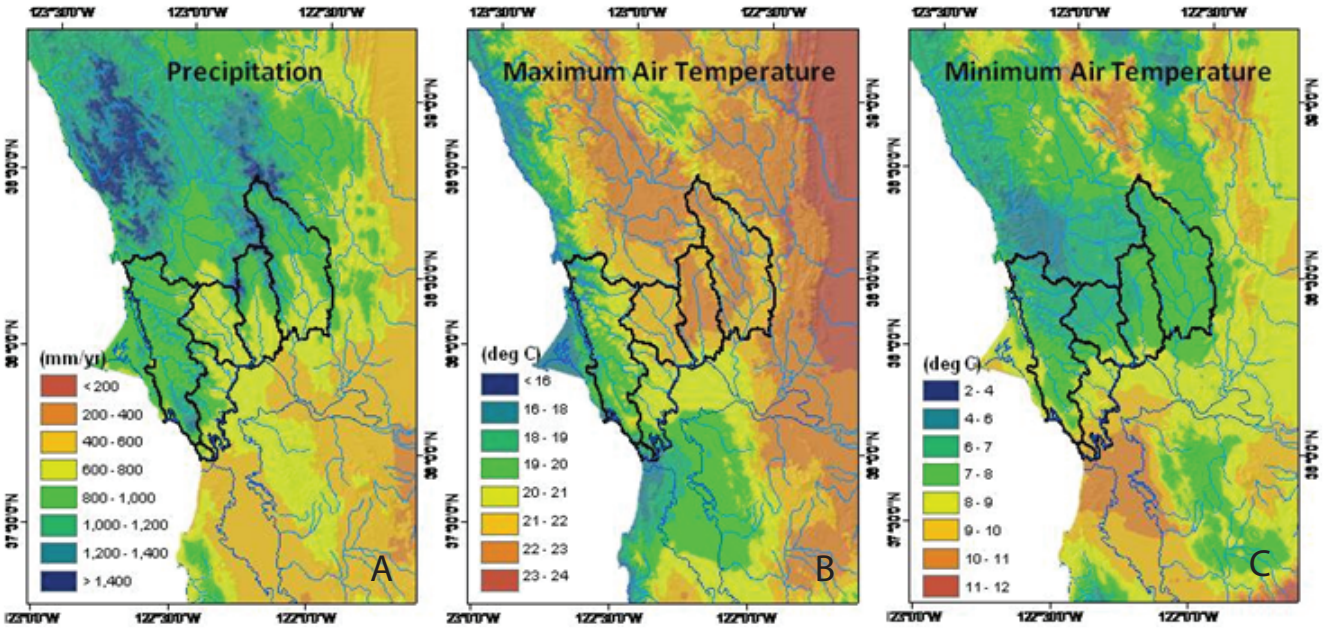


**Figure 4A–C** Average annual precipitation and maximum and minimum temperatures, North Bay region, 1971–2000

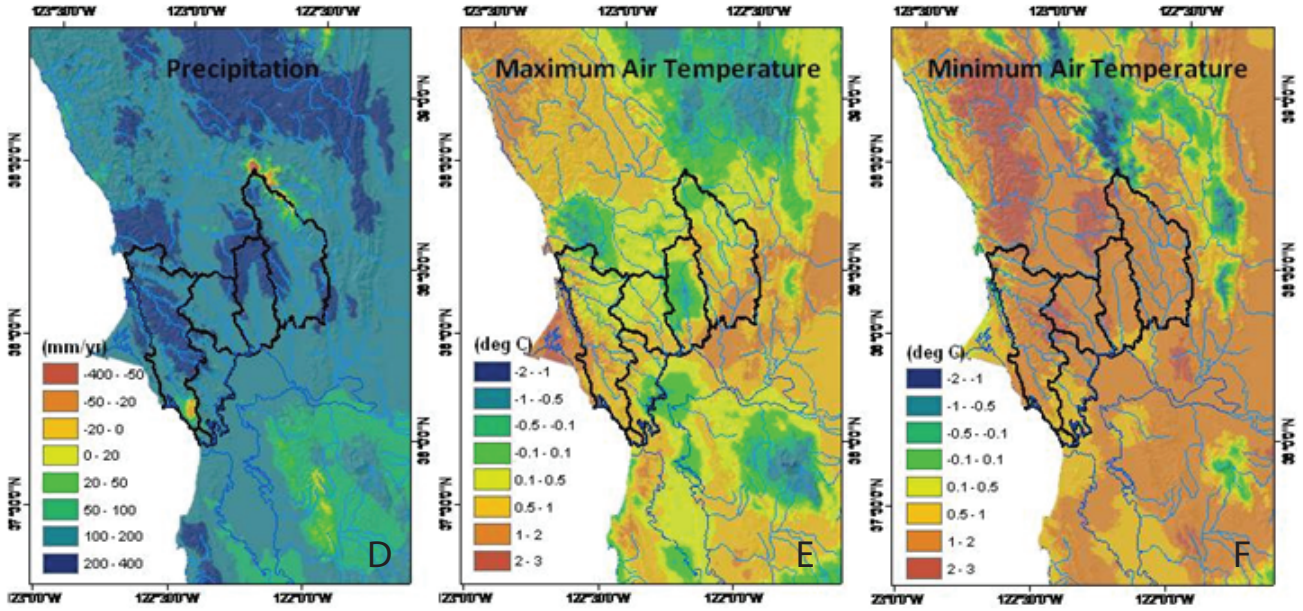


**Figure 4D–F** Direction and magnitude of change in annual average precipitation and maximum and minimum temperatures, North Bay region, 1971–2000

Trend analysis for precipitation and temperature across North Bay region based on monthly PRISM data downscaled to 270 m for 1971–2000. Series A–C shows average annual values and series D–F shows total change for this time-period. Major basins are delineated in black outline. A–C display a decreasing precipitation gradient from the coast and montane headwaters to inland valleys, an increasing gradient in maximum temperatures from coast (18 °C to 19 °C) to inland (22 °C to 23 °C), and relatively consistent trends across the region in minimum temperatures. Series D–E display an increase of approximately 50 to 200 mm in precipitation, a variable trend in maximum temperatures, and more intensive increases in minimum temperature (on the order of 1 °C to 2 °C) across the region.

an average rate of change of 0.014 °C $y^{-1}$. During this historical period there has also been a trend towards increasing precipitation: for the first half of the century (1900–1950), annual precipitation averaged 752 mm $y^{-1}$, versus an average of 845 mm $y^{-1}$ (1951–2010)—(12% greater)—for the latter half of the century.

Mapped trends in precipitation and air temperature over the historical record for this area reveal the spatial variability underlying average regional values. Figure 4A shows the spatial distribution of average values for monthly precipitation, monthly maximum air temperature ($T_{max}$), and monthly minimum air temperature ($T_{min}$) for 1971–2000. High spatial variability is a product of coastal marine influences combined with variable topographic relief, which in turn creates topographic shading effects, cold air drainage, variation in adiabatic lapses in air temperature, and other controls on fine-scale climate.

Figure 4B displays the significant spatial variability in patterns of total change in climate over the same time-period. Patterns of change show how localized areas of increases and decreases in precipitation and temperature are not uniform over the study area—variability which informs the interpretation of future projections. Trends in air temperature have been mostly warming, particularly over valley bottoms, while some zones of montane headwaters have experienced a cooling trend. The rate of change in minimum temperatures exceeds that for maximum temperatures, pointing to a recent trend toward warmer nighttime and winter temperatures. The spatial distribution of change in climate is variable over the area, with some locations changing more than others, which suggests that topographic features are influencing local climates in a manner that should be taken into account in projecting future climates.

## Regional Temperature and Precipitation Scenarios Derived from General Circulation Models

By combining historic data derived from PRISM with projected temperature and precipitation values for four future scenarios, we can compare model outputs with both the historic record and each other. Figure 5A-B displays comparable amounts of predicted warming for the GFDL and PCM models for both emissions scenarios, but distinctly different precipitation signatures between GFDL and PCM models. The PCM model projects a significantly "wetter" future scenario than historic conditions or GFDL projections.

There is an insignificant separation between the GFDL and PCM models in average maximum temperatures projected by the century's close (2091–2100) for both the A2 (25.1 °C and 24.8 °C, respectively, with a resultant average of 25.0 °C for A2 scenarios) and the B1 (23.9 °C, both models) (Figure 5A). For the B1 scenarios this represents a rate of change of approximately 0.021 °C $y^{-1}$ (1.5 times the 20th century rate of change) and for the A2 scenarios, this results in a rate of change of approximately 0.032 °C $y^{-1}$ (2.3 times the 20th-century rate of change). While there is some variation in slope, the total change over time is relatively steady. This series demonstrates a close alignment between the GFDL A2 and PCM A2 scenarios and between the GFDL B1 and PCM B1 scenarios in terms of temperature projections, despite variations between decades.

Figure 5B shows that projected precipitation is highly variable in terms of projected long-term trends. In contrast to temperature projections, which are driven by differences in emissions scenarios (which are not significantly different until 2050 and then diverge by the end of the century), model algorithm (GFDL versus PCM) is more important than emissions scenarios in driving projected precipitation. Hence, while temperature and precipitation both depend on large-scale mechanisms, precipitation is more sensitive to model assumptions, and, is therefore, more uncertain in general, because of model physics. Compared to the 20th century average of 799 ± 280 mm $y^{-1}$ (1901–2000), the average precipitation for the two GFDL scenarios (2001-2100) is 819 mm $y^{-1}$ (2% greater than 20th century) while the average precipitation for the two PCM scenarios (2001–2100) is 918 mm $y^{-1}$ (15% greater than 20th century). While century-scale averages remain in the range of historic variability, values projected for individual decades display unprecedented wet and dry periods. The B1 scenarios for both models project unprecedented annual peaks in the first half of the century (GFDL B1 projects 1,088 ± 179 mm $y^{-1}$ for 2011–2020, PCM B1 projects

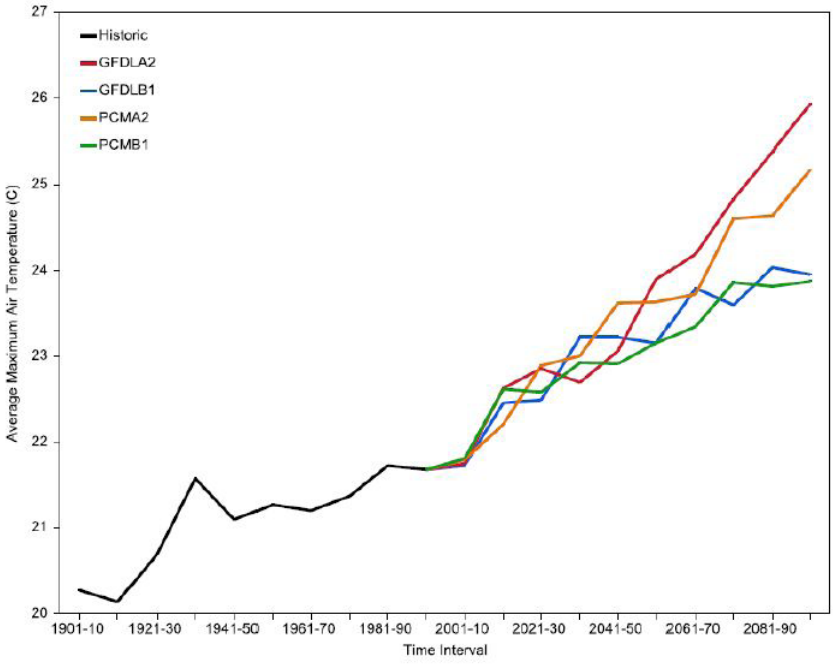


**Figure 5A** Historic (1901–2000) and GCM-projected (2001–2100) maximum temperatures

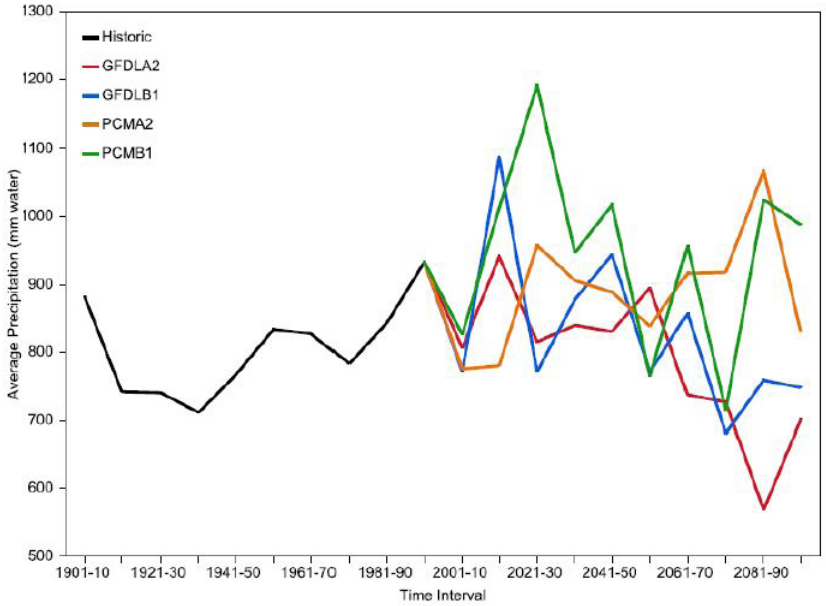


**Figure 5B** Historic (1901–2000) and GCM-projected (2001–2100) precipitation

General Circulation Model (GCM) temperature and precipitation outputs downscaled to North Bay region based on monthly values averaged over decade intervals. Historic values derived from PRISM. Projected data series (2001–2100) represent four combinations of GCM model (GFDL or PCM) and emissions scenario (A2 "business as usual"or B1 "mitigated') as identified in legend.

1,192 ± 181 mm $y^{-1}$ for 2021-2030). By the next century's close, the GFDL and PCM models diverge, with the greatest contrast in 2081–2090 when the GFDL A2 projects an unprecedented drought averaging only 569 ± 80 mm $y^{-1}$ while for the same period the PCM A2 projects 1,067 ± 188 mm $y^{-1}$.

By the century's close, the four scenarios may be distinguished by emissions scenarios that define two different temperature futures (A2 and B1, as listed above) and a range of potential precipitation projections, depending on whether the GFDL or the PCM model is applied. By the 2091–2100 time interval, the wetter–warmer PCM model for the A2 and B1 scenarios is characterized by an average precipitation value of 910 ± 115 mm $y^{-1}$ (14% more than the 20th-century average), versus a warmer–drier GFDL model average for the A2 and B1 scenarios of 725 ± 79 mm $y^{-1}$ (9% less than the 20th-century average). This is the basis for terming GFDL projections "warmer–drier" versus PCM projections as "warmer–wetter" in proceeding sections.

## Basin Characterization Model Results: Future Hydrology Scenarios

Figure 6A–N displays time series data (with average values based on monthly values) for the GFDL A2 and PCM A2 scenarios for the last and current centuries in 30-year intervals (the exception is the 1896–1910 interval, which represents only 25 years). Plots thus combine historic data for the last century with projected data for the next, starting in 1896 and closing in 2100. These results are summarized in Table 3, which also displays values for B1 emissions scenarios not shown in Figure 6A–N. Values displayed from

1896 to 2000 are derived from PRISM; while values from 2000 to 2100 are a combination of GCM outputs for temperature and precipitation (summarized above) and modeled BCM outputs for hydrologic variables. The left sides of Figure 6A–N display annual data distributions for 30-year intervals, including box plots scaled vertically to the standard deviation, and with "whiskers" scaled to the 5% to 95% confidence interval. The right side of the data plots show the frequency distribution of annual values compiled for each 30-year time interval.

### *Trends in Runoff and Recharge*

Under both projected scenarios (GFDL A2 and PCM A2), histograms of annual precipitation values shown in Figure 6E–F show a wide distribution relative to historic conditions, with unprecedented annual extremes (represented by maxima in excess of 2,000 mm $y^{-1}$) and a concentration of the remainder of events in the lower range of the historic record. This indicates a shift away from the historic distribution where the centroid of the distribution is concen-

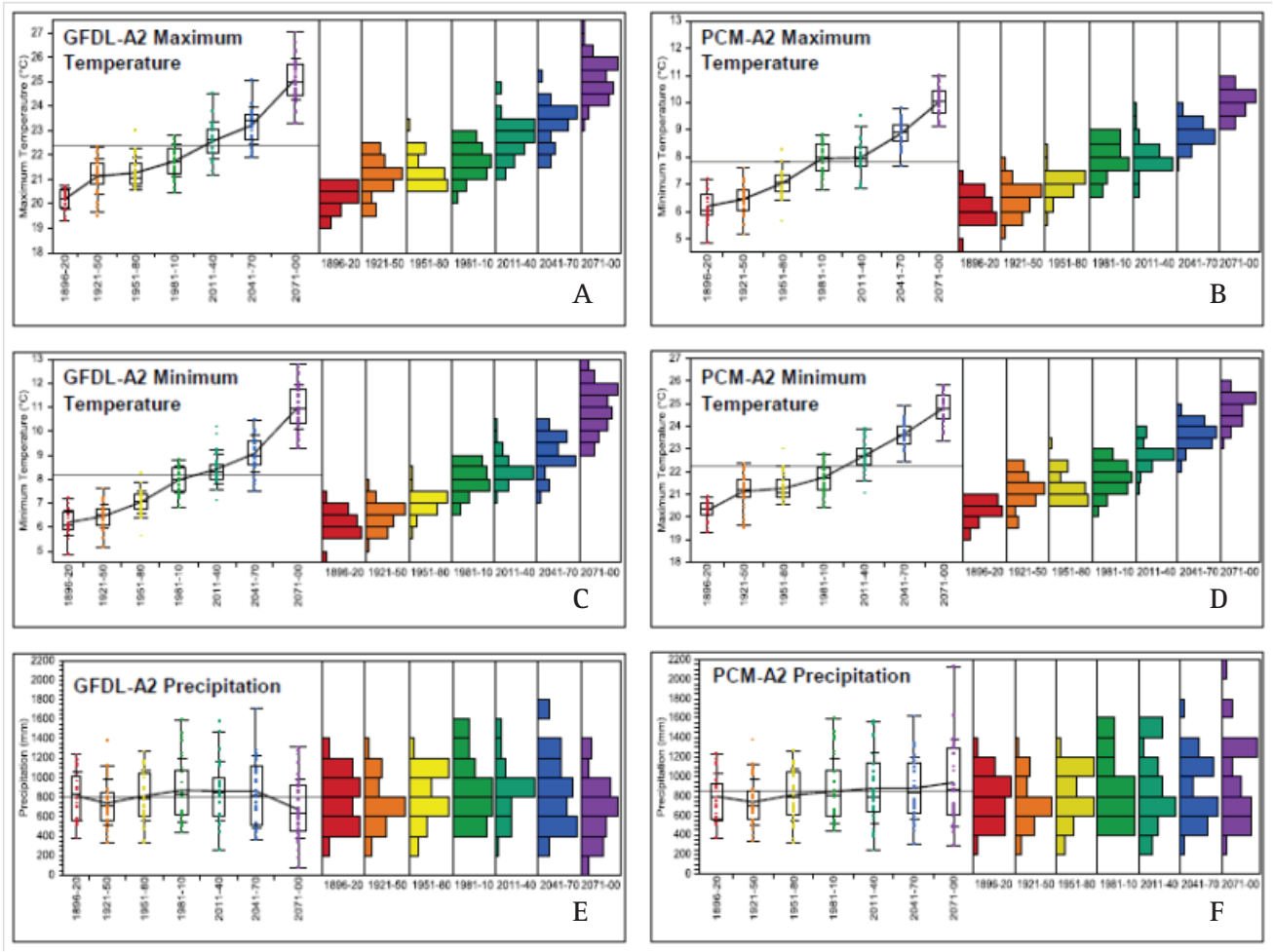


**Figure 6A–F** Historic values (1896–2009) for temperature and precipitation, North Bay region, derived from PRISM; projected values for temperature and precipitation derived from downscaled GCMs (GFDL A2 "warmer–drier" and PCM A2 "warmer–wetter" scenarios, 2010–2100). Box plots represent 30-year intervals: the mid-line is the median, the box shows the 25th and 75th quartiles, the next lines are the standard deviations, and the end whiskers represent outliers within 1.5 times the interquartile range.

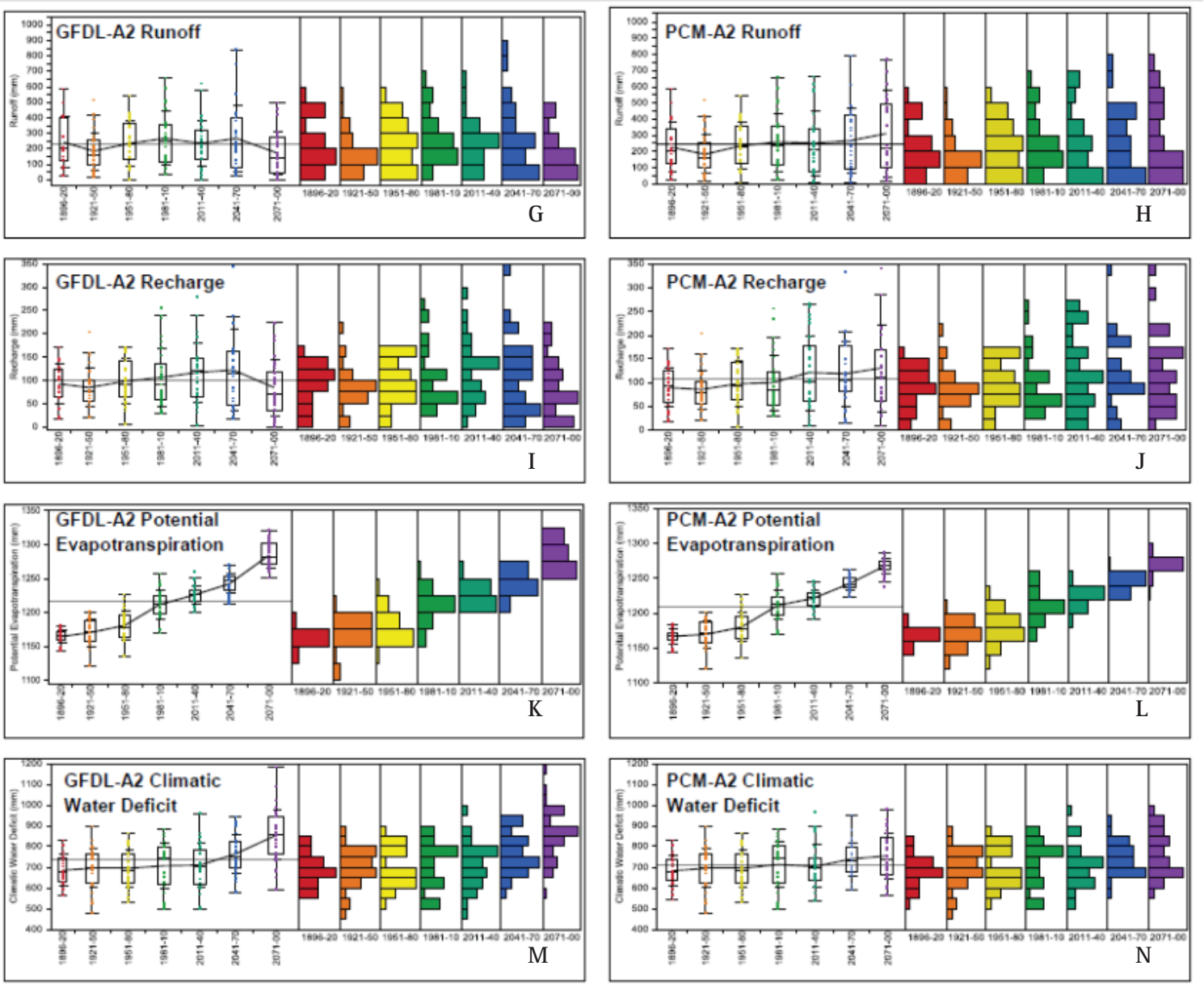


**Figure 6G–N** Historic (1896–2009) and projected (2010–2100) hydrology, BCM estimates, North Bay region, GFDL-A2 and PCM A-2 scenarios. Hydrologic parameters of runoff (G–H), recharge (I–J), evapotranspiration (K–L), and water deficit (M–N) are derived from Basin Characterization Model (BCM) simulations using PRISM data for historic values (1896–2009) and using downscaled GCMs (GFDL A2 "warmer–drier" [G, I, K, M] and PCM A2 "warmer–wetter" [H, J, L, N]) for future projections (2010–2100). Box plots represent 30-year intervals and are sized to the standard deviation, "whiskers" define the 5% to 95% confidence interval, and histograms show the frequency distributions of average annual values.

trated around the mean of record, with a dominance of relatively moderate annual average precipitation values (approximately 800 ± 250 mm $y^{-1}$). The response of hydrologic variables including runoff and recharge is highly sensitive to variation in precipitation over time and between scenarios. The diversity of estimated precipitation regimes across the suite of four scenarios shown in Figure 7 implies that a broad range of possible combinations of temperature and precipitation are modeled in the course of this study. The trend of spreading the width of distributions towards formerly rare or even unprecedented precipitation extremes drives variability in runoff and recharge for all scenarios.

Distributions of average annual values for runoff (Figure 6G–H) for both scenarios mirror the increasing spread of precipitation values, indicating more extreme events at both ends of a range that includes unprecedented extreme wet values for average annual runoff compared to a 20th-century average of 227 ± 154 mm $y^{-1}$ (1901–2000). For the GFDL A2 scenario, by this century's close (2071–2100), estimated annual average runoff is 187 ± 27 mm $y^{-1}$ (18% lower than the 20th-century average). For the PCM A2 scenario, by this century's close (2071–2100), average annual runoff is estimated at 313 ± 50 mm $y^{-1}$ (38% higher than the 20th-century average).

For recharge, we estimate nearly a 25% increase in rates over the period ranging from 1921–2010. Figure 6I–J shows that both models project increases in the first half of the next century in response to increased precipitation. However, the full distribution of average annual values trends towards more frequent occurrences of low-recharge years with infrequent high-recharge years. Paralleling runoff, this distribution includes more extreme annual events, compared to the more consistent pattern of annual values concentrated around the mean of record observed in historic time steps. For the GFDL A2 scenario, by this century's close (2071–2100), estimated average annual recharge is 89 ± 10 mm $y^{-1}$ (6% lower than the 20th-century average). For the PCM A2 scenario, by this century's close (2071–2100), average estimated recharge is 131 ± 17 mm $y^{-1}$ (39% higher than the 20th-century average).

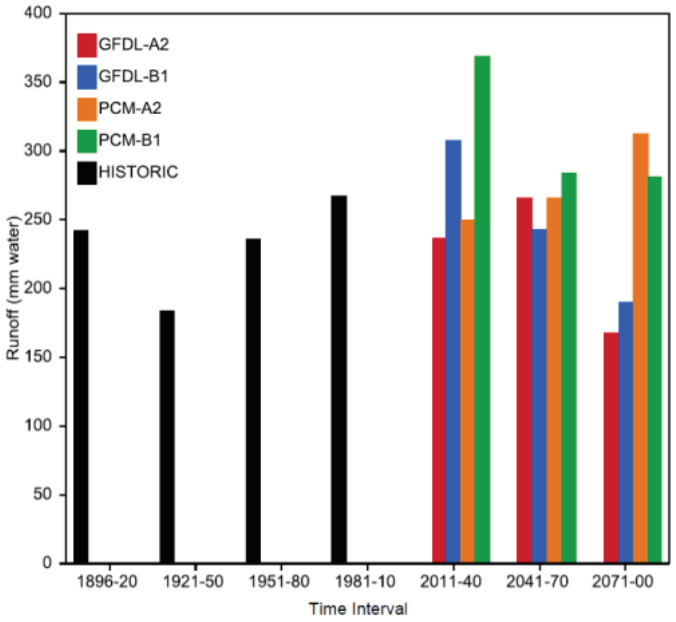


**Figure 7** A comparison of historic (1896–2009) to projected (2010–2100) average annual runoff for four future climate scenarios, North Bay region. Each bar represents average annual runoff estimated by the BCM for the North Bay region (NBWA jurisdiction) over the defined time interval, with black bars derived from PRISM data (1896–2009), and colored bars derived from GCM projections. For the three projected time periods, the first (2011–2040) shows a case where the B1 scenarios are significantly wetter than the A1 scenarios, the second (2041–2070) shows a case where all scenarios are comparable in terms of projected runoff, and the third (2071–2100) demonstrates a case where the PCM projections are significantly wetter than the GFDL projections for both emissions scenarios.

### *Trends in Evapotranspiration*

Figure 6A–B shows an increasing trend in temperature of approximately 0.03 °C $y^{-1}$ (between the 1981–2010 and 2071–2100 time intervals), which in turn drives increases in estimated PET shown in Figure 6K–L. While the 20th-century rate of change for PET was approximately 0.22 mm $y^{-1}$, the A2 scenarios project PET to increase at a rate of approximately 0.56 to 0.74 mm $y^{-1}$. The net effect of the accelerated rate of change in PET from temperature forcing is that, by next century's close (2071–2100), average PET is projected to range from 1,268 mm $y^{-1}$

(PCM A2) to 1,286 mm $y^{-1}$ (GFDL A2). The entire span of annual values projected for 2071 to 2100 exceed the distribution of annual values for the first historic time interval (1896–1920). This amounts to an increase on the order of 7% to 8% (compared to the 20th-century average) in average annual PET (approximately 100 mm of water or 13% of 20th-century average annual precipitation), for both drier and wetter scenarios.

### *Trends in Climatic Water Deficit*

Climatic water deficit (CWD) is projected to increase over this century at a rate ranging from 0.25 to 1.5 mm $y^{-1}$, depending on whether a wetter or drier scenario is used (PCM B1 and GFDL A2, respectively). For the PCM A2 scenario, by this century's close (2071–2100) average estimated CWD is 758 ± 20 mm $y^{-1}$ (8% higher than the 20th century average). For the GFDL A2 scenario, by this century's close (2071–2100), average estimated CWD is 855 ± 19 mm $y^{-1}$ (21% higher than the 20th-century average). Thus, while the wetter scenario projects a 15% increase in precipitation and runoff compared to historical (20th-century) conditions, this additional water does not offset drought stress to soils, and, as a result, there is still a soil drying trend on the order of 50% of the effect estimated for the lower precipitation scenario.

### *Trends in Water Balance Partitioning*

Figure 8 shows partitioning of the water balance over time. Visually subtle variations shown here have significant effects in terms of determining whether watersheds experience drought versus

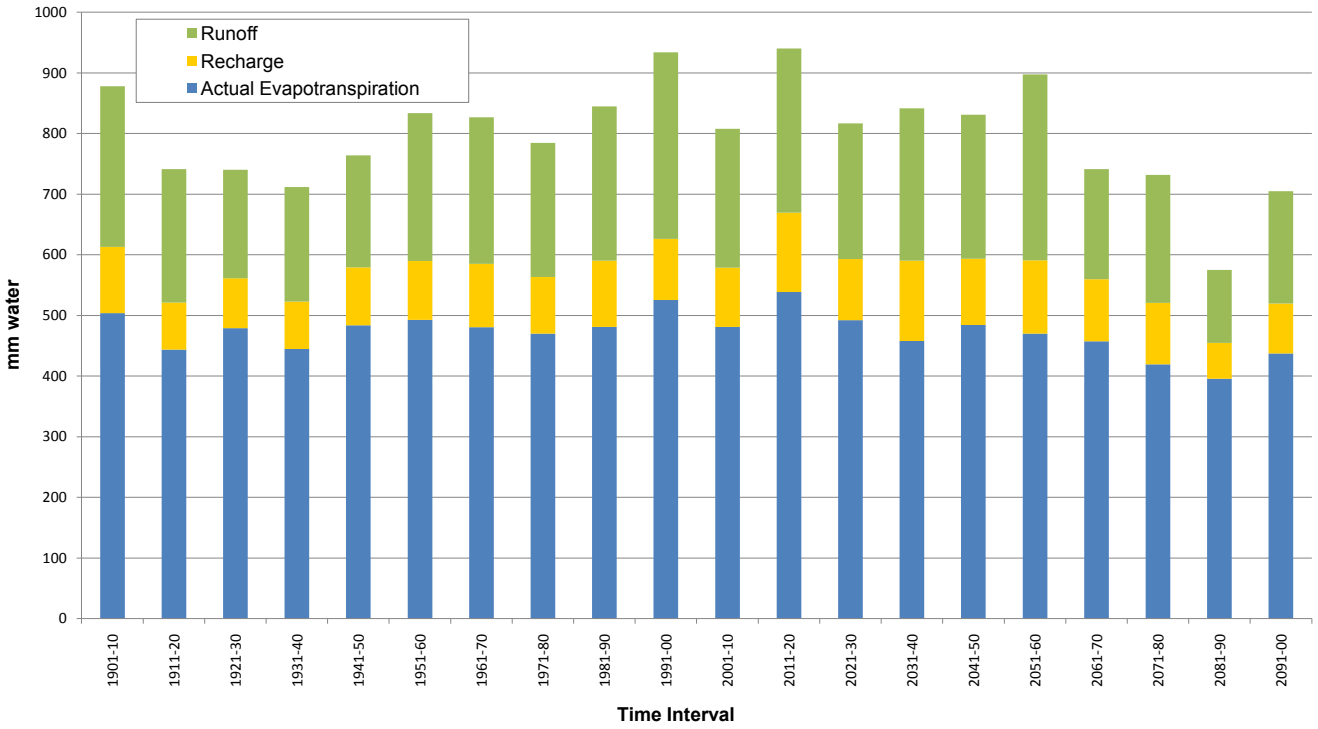


**Figure 8** Historic (1896–2009) versus projected GFDL A2 "warmer–drier" scenario (201–2100) water balance partitioning for the North Bay region, using monthly data averaged over decade intervals. Histograms displaying water balance partitioning between runoff (green), recharge (yellow), and evapotranspiration (blue) show that in low water years, proportionally more water is converted to evapotranspiration, versus during high water years, when proportionally more water is available for recharge and runoff.

adequate water supply, underscoring that small trade-offs (5% to 10%) between water balance terms can have big effects in terms of watershed condition. For an average decade shown here, the sum of plotted terms is 797 mm (equivalent to precipitation plus change in soil storage, with soil storage typically on the order of 1% to 3% of the water balance), with approximately 59% in AET, 12% in recharge, and 28% in runoff. Note that for the wettest decade shown here, the sum of plotted terms is 940 mm, with approximately 57% in AET, 14% in recharge, and 29% in runoff, which are relatively close to the average values. By contrast, for the driest decade on record, the sum of the plotted terms is 575 mm, with approximately 69% in AET, 10% in recharge, and 21% in runoff. Thus, as conditions trend toward those typified by the driest decade predicted here, a larger fraction of the total water available is "lost" to evapotranspiration, leaving approximately 10% less water (on the order of 60 to 90 mm water per year) available for recharge and runoff.

## Projected Spatial Distribution of Runoff, Recharge, and Climatic Water Deficit

The sequence of maps shown in Figure 9A–F depicts the percentage change in runoff, recharge, and CWD calculated between the average of 1971–2000 and the average of 2071–2100 for the GFDL and PCM models for the A2 scenario. Represented average values are plotted at the scale of minor basins. The resilience of individual minor basins to future changes in climate is a function of interactions among topography, solar orientation, soils, and geology. These maps illustrate the relative vulnerability and resilience of the various minor basins to future changes in climate by the relative changes over the 100-year period. The most notable difference among the maps is between models, with the PCM model projecting less drought stress than the GFDL model. Spatial trends reflect the moderating effect of coastal marine climates, with lower changes in the future for all variables, especially the CWD, for basins located nearer to the coast. Minor basins characterized by thick alluvium over valley bottoms provide both the opportunity for greatest recharge and risk of greatest CWD. An understanding of the variability between minor basins can help to characterize hydrologic response at a scale useful for management.

## Projected Climate Change Effects on Stream Flow and Basin Recharge

Stream flow and estimated basin recharge integrates many responses of the basin to variation in climate. Evaluating patterns of basin discharge or stream flow over time, at the scale of a 3-year running average, helps to discern potential future frequencies of both wet periods and drought. These analyses can be conducted at the scales of the region as a whole, for a river (major) basin at a gauged location, or for a minor basin (sub-watershed). In this section, we demonstrate analyses that can be conducted using study results at all three scales.

BCM simulations enable stream discharge data to be viewed as a time series. We chose to display discharge as a 3-year running average to be consistent with what water agencies typically use to evaluate potential drought conditions (with a drought typically considered to comprise three contiguous dry years). Figure 10A displays effects on runoff available for stream flow at the scale of the entire region, and Figure 10B represents historic and projected stream flow for the Napa River at the St. Helena gage in terms of 3-year running averages.

Figure 10A shows that for the region as a whole, annual amounts of runoff available as stream discharge averaged $452 \times 10^6$ m$^3$ during the 20th century. For this century, the GFDL A2 scenario estimates an average of $445 \times 10^6$ m$^3$ runoff available for streamflow (2% less than the 20th-century average): the PCM A2 estimates $539 \times 10^6$ m$^3$ runoff available for streamflow (19% more than the 20th-century average) based on mean 3-year running average values.

Figure 10B shows that for the Napa River at St. Helena, the historic record (1940–2007) displayed a mean 3-year running average value of $10.4 \times 10^6$ m$^3$. The GFDL A2 scenario averaged $10.1 \times 10^6$ m$^3$: the PCM A2 scenario averaged $13.7 \times 10^6$ m$^3$. The PCM A2 series includes eight 3-year average values that exceed the maxi-

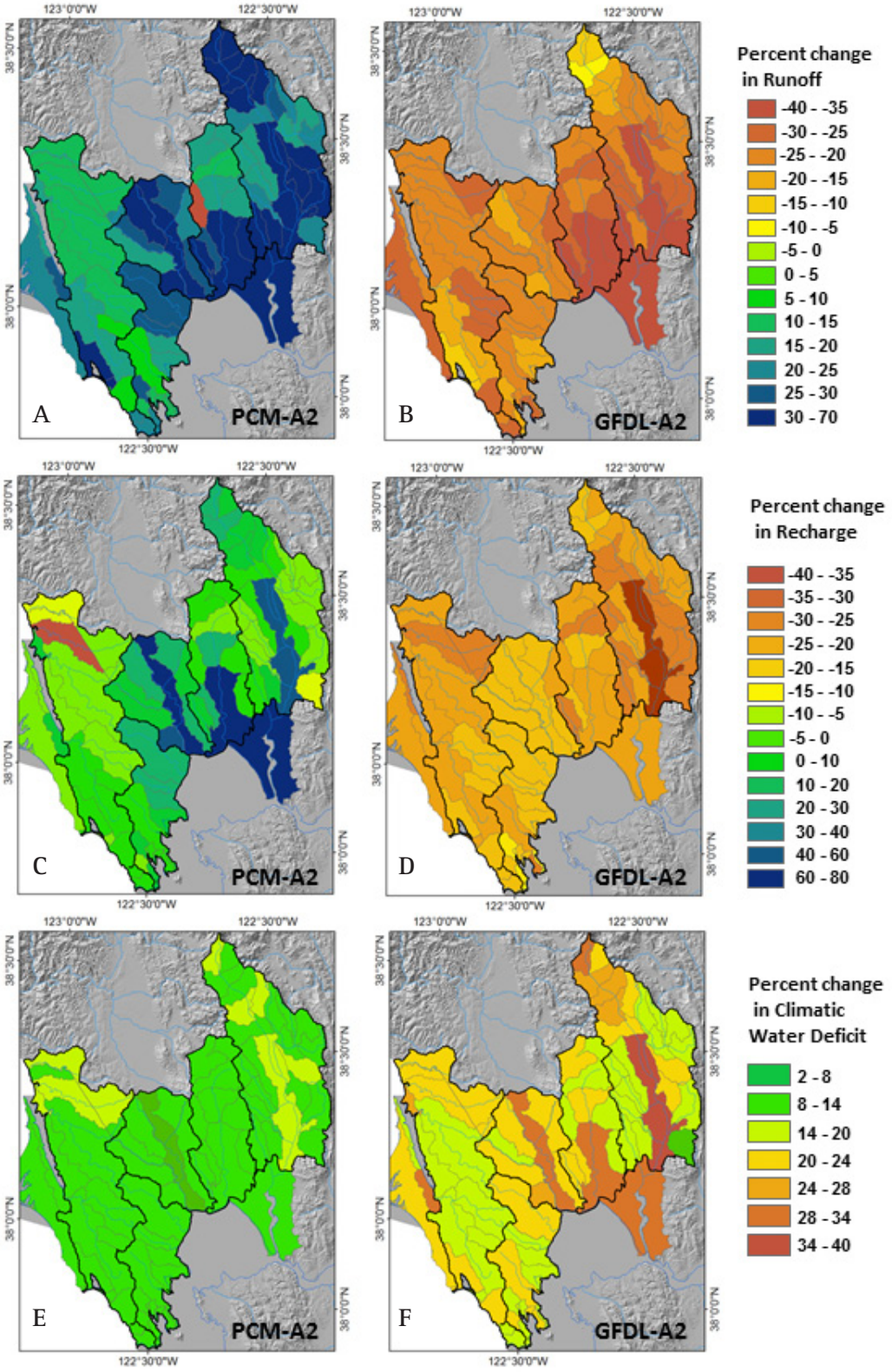


**Figure 9A–F** Spatial distribution of projected climate impacts on hydrology estimated using Basin Characterization Model (BCM), North Bay region. Maps A–F display the diversity of potential hydrologic response to climate change within major basins by showing the spatial distribution of differences between the 1971–2000 and 2071–2100 time intervals. A–B displays runoff, C–D displays recharge, and E–F displays water deficit for the PCM A2 "warmer–wetter" scenario (A, C, E) and the GFDL A2 "warmer–drier" scenario (B, D, F). 270-m grid results are averaged for sub-basins. In general, valley bottoms typified by thick layers of alluvium show the greatest magnitude of potential change because of storage capacity. While runoff and recharge generally trend in opposite directions for the two models (in the positive direction for PCM and in the negative direction for GFDL), both models predict increases in water deficit that range from 8% to greater than 34%.

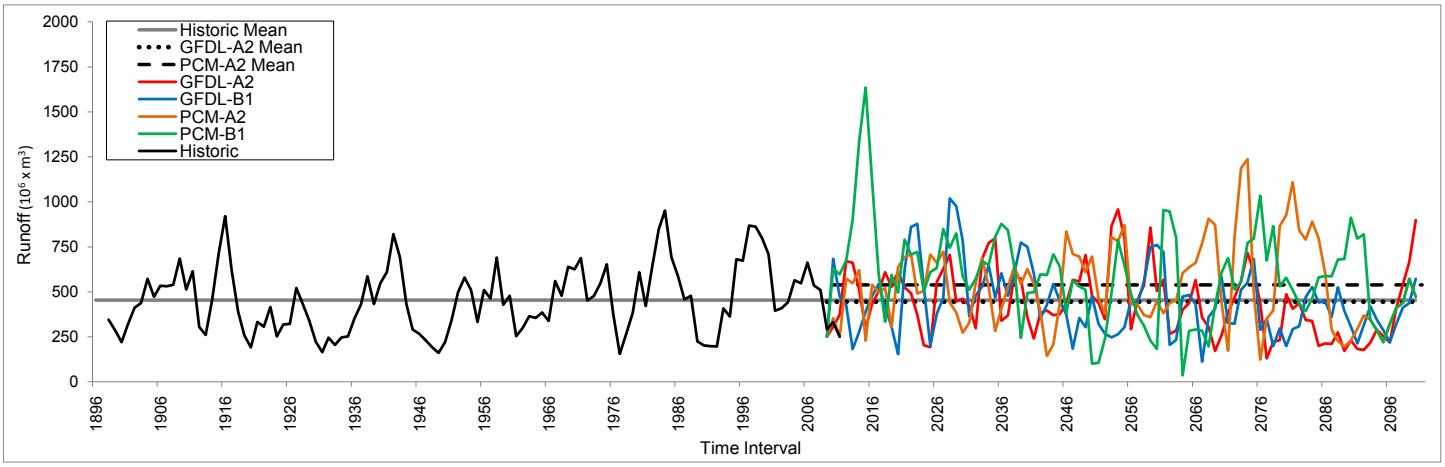


**Figure 10A** Historic estimated runoff (1896–2009, derived from PRISM data) and projected runoff (2010–2100) for four scenarios in the North Bay region (excludes Marin Coast planning basin). Plot shows increased future variability in 3-year running average for all scenarios.

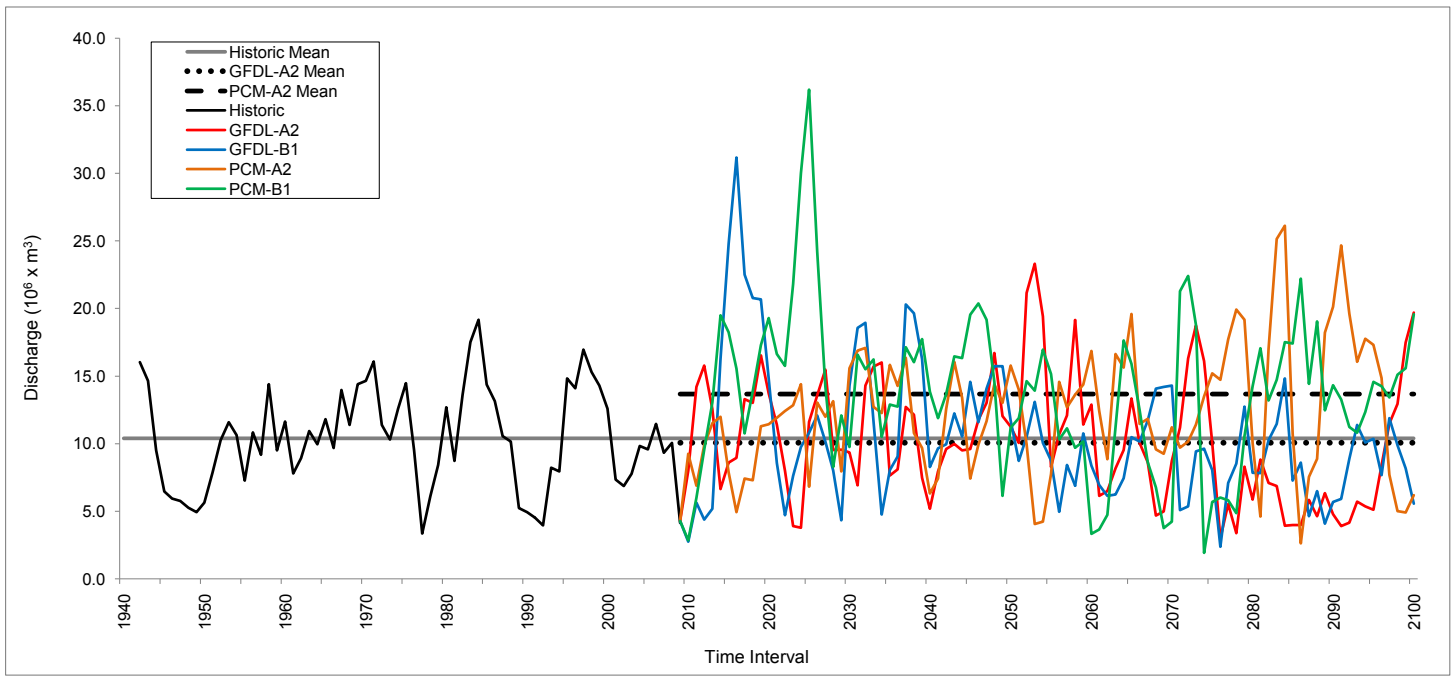


**Figure 10B** Historic stream discharge (1896–2009, derived from USGS gage data) and projected stream discharge for four scenarios for USGS gage on Napa River at St Helena, #1145600. Plot displays increased future variability in 3-year running average for all scenarios, and trend towards end of current century for more discharge under PCM compared to GFDL scenarios.

mum 3-year average value of the historic record ($19.2 \times 10^6$ m$^3$). The GFDL A2 series includes three 3-year average values that exceed the maximum 3-year average of the historic record, and one 3-year average value that is less than the minimum 3-year average of the historic record ($3.4 \times 10^6$ m$^3$). In terms of underlying annual values for stream discharge, the GFDL A2 scenario displays that for 15 out of 90 years flows would be below the previous annual minimum of record.

River managers and engineers typically rely on frequency plots of cumulative discharge to size hydraulic structures and stream channel restorations. Figure 11 shows the cumulative probability of annual stream discharge for the Napa River at St. Helena with a historic frequency curve (1971–2000) compared to estimated values under the GFDL A2 and PCM A2 scenarios (2071–2100). This plot shows that future scenarios project shifts in the negative direction under GFDL A2, and shifts in the positive direction for PCM A2. For example, if one examines values estimated for a return frequency of 0.5, which estimates the average discharge of the system, the historic value is $93.7 \times 10^6$ m, versus a projected value of 65.3 x $10^6$ m3 for the GFDL A2 scenario, and a projected value of $110.2 \times 10^6$ m$^3$ for the PCM A2 scenario.

Frequency plots can also be created using 3-year average discharge and recharge values to show managers potential shifts in discharge frequencies for minor planning basins. Figure 12 shows vertical histograms that compare runoff available for stream discharge and estimated basin recharge for

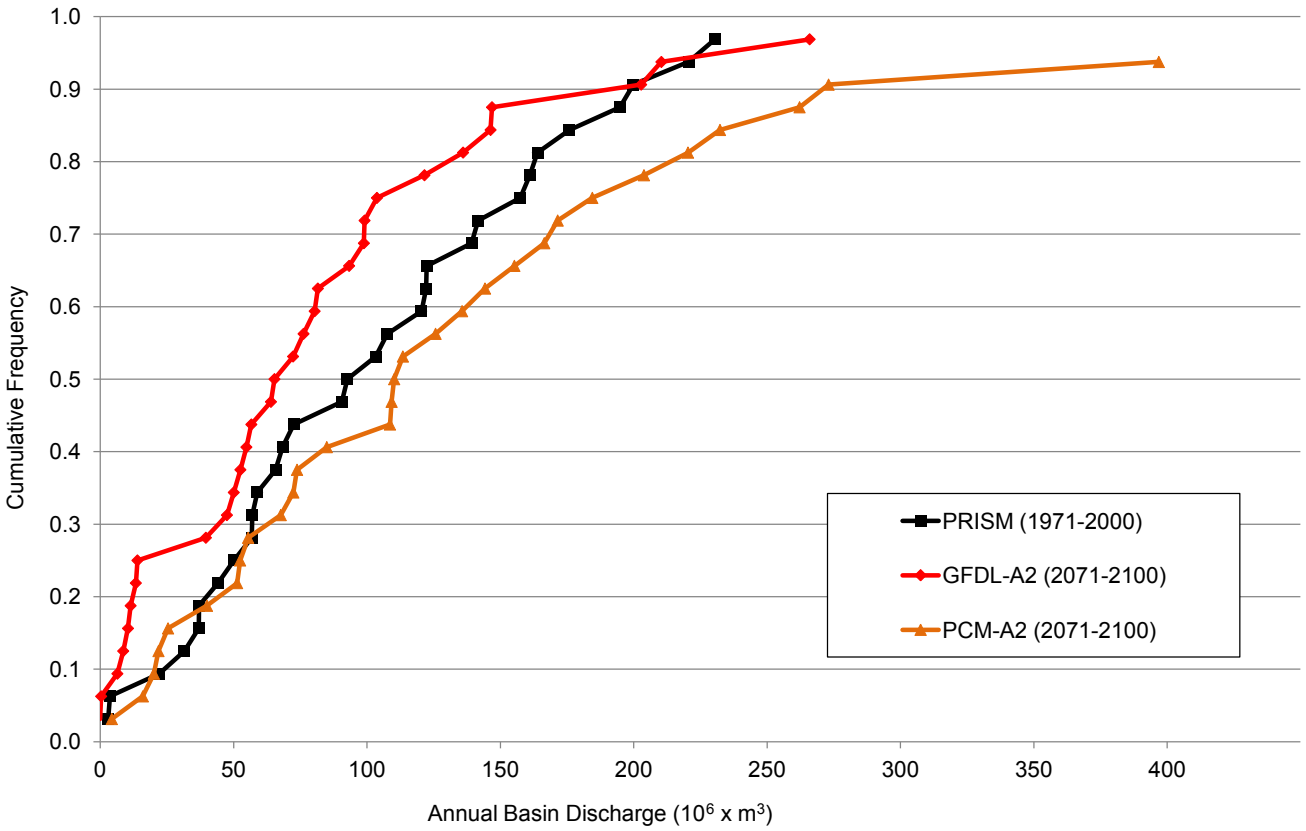


**Figure 11** Historic (1971–2000) versus projected (2071–2100) cumulative probability of annual stream basin discharge, Napa River at St. Helena. Black squares represent historic conditions (1971–2000), derived from USGS gage data), red diamonds represent projected GFDL A2 scenario (2071–2100, BCM simulation), and gold triangles represent projected PCM A2 scenario (2071–2100, BCM simulation).

the minor basin of the Napa River known as Milliken Creek. This plot shows that available runoff exceeded 1,000 × $10^3$ $m^3$ 57% of the time from 1971 to 2000. Under the GFDL A2 scenario for 2071–2100, this threshold would be exceeded only 23% of the time. In terms of basin recharge, while for the historic period (1971–2000) basin recharge exceeded 500 × $10^3$ $m^3$ 74% of the time, under the GFDL A2 scenario for 2071–2100, this threshold would be exceeded only 36% of the time.

## Projected Climate Change Effects on Timing of Water Availability

The BCM generates monthly estimates for all hydrologic parameters, which facilitates an examination of how climate change potentially affects hydrologic seasonality. Figure 13A–D compares average values by month for precipitation, runoff, recharge, and PET for recent conditions (1981–2010) and projected conditions under GFDL A2 and PCM A2 (2071–2100). Both projected scenarios display significant reductions in early wet-season rainfall, and while PCM A2 projects significantly higher rainfall in January, February, and March, it joins the GFDL A2 scenario in projecting drier conditions in April, May, and June than for the recent time-period (Figure 13A). This pattern is reiterated in seasonal patterns of runoff and recharge (Figure 13B–C). Figure 13D shows that both future scenarios show increased PET during May through September, which is likely to increase water demand regardless of variations in rainfall during antecedent winter months.

## Comparative Analysis of Major North Bay Basins

Appendix B provides model outputs calculated for the five major basins of the North Bay for all variables analyzed using the BCM for the historic (1896–2009) and projected (2010–2100) time-periods. Appendix B shows that in terms of temperature, there is an approximate 0.5 to 1.0 °C separation between each major basin, except for the combined set of Sonoma and Napa (which are highly similar), in terms of maximum temperatures. For minimum temperatures, Marin Bay emerges as consistently on the order of 1.0 °C warmer than the set of the remainder of basins

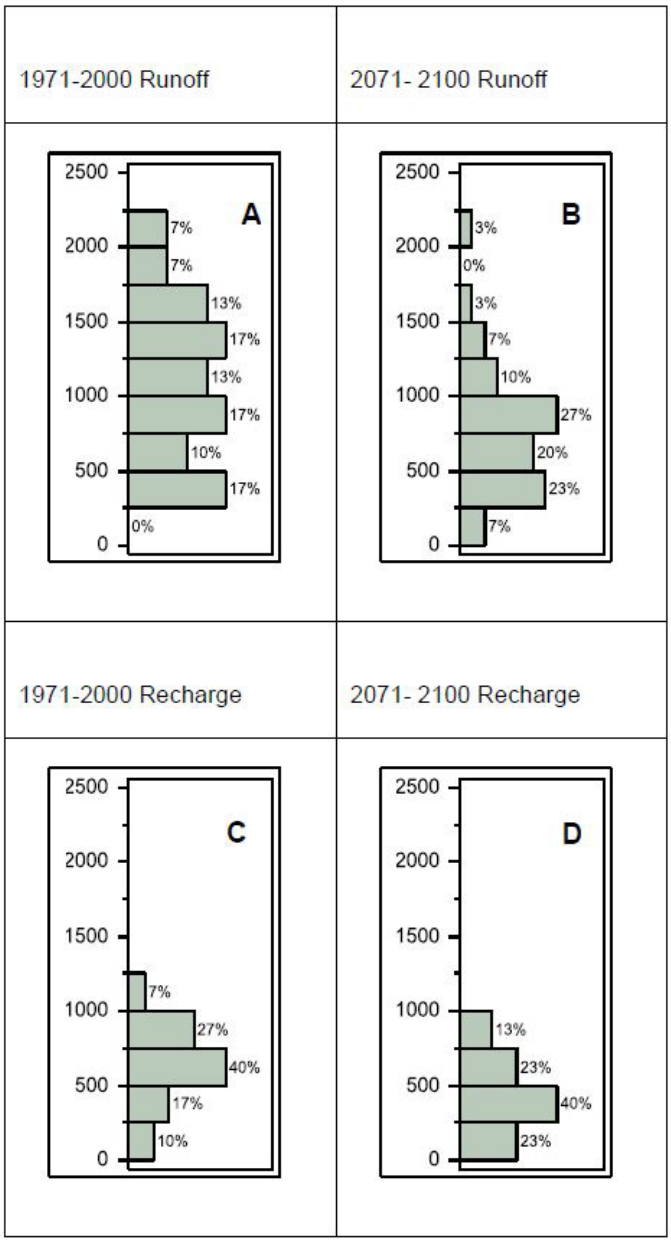


**Figure 12A–D** Three-year running average histograms for runoff (A–B) and recharge (C–D) for Milliken Creek sub-basin. Frequency distributions compare historic (1971–2000, from USGS gage data) and projected (2071–2100, from BCM simulation for GFDL-A2 scenario) values. Percent labels show total frequency of values for each histogram interval. Units are $10^3$ x $m^3$ of water.

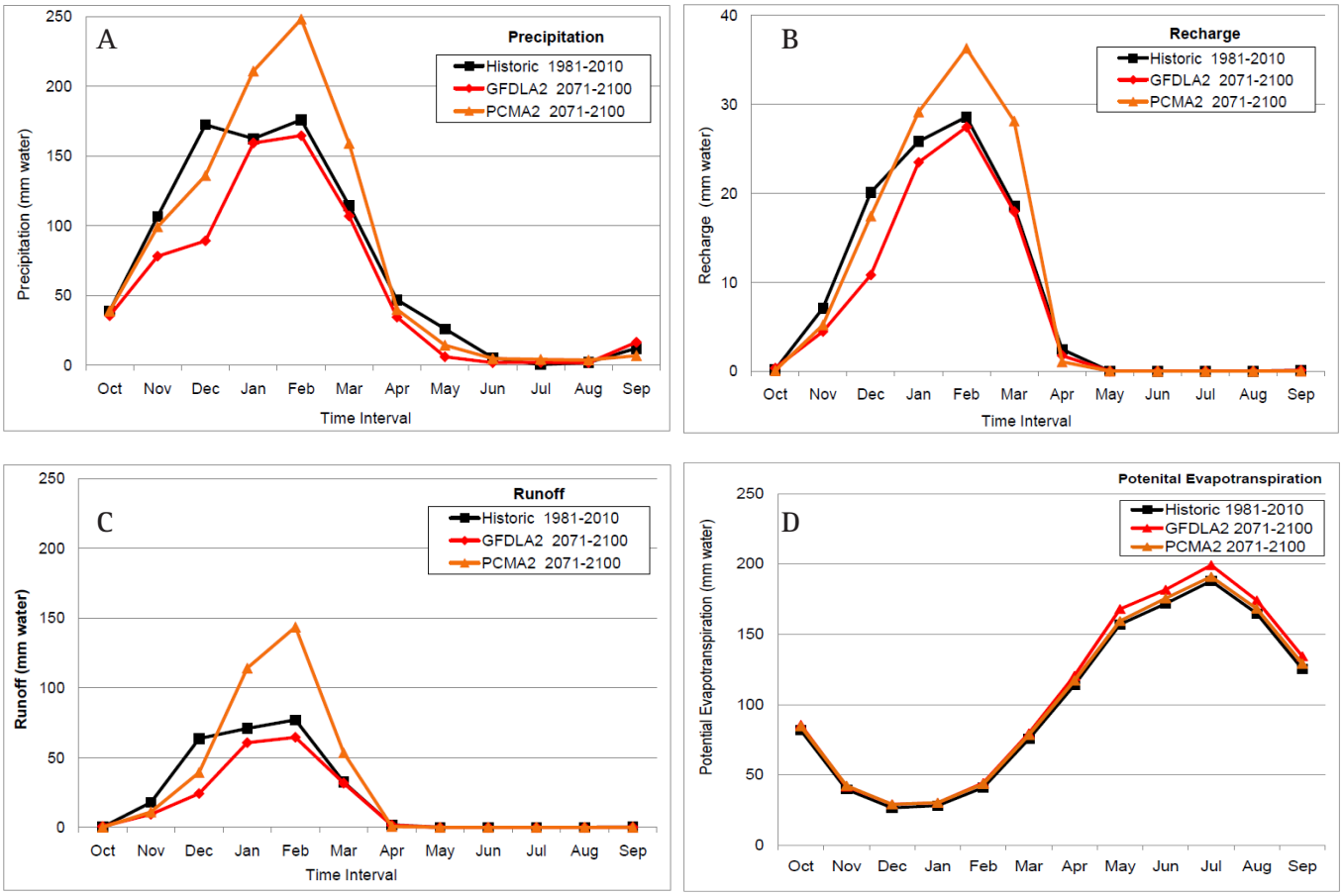


**Figure 13A–D** Projected climate effects on seasonality of climate hydrology parameters, North Bay region. Each plot compares recent (1981–2010) versus projected (2071-2100) monthly average values for individual months of water year for (A) precipitation, (B) runoff, (C) recharge, and (D) potential evapotranspiration. Black squares show recent values (derived from PRISM), red diamonds shows projected "warmer–drier" scenario (GFDL A2 scenario, 2071–2100, BCM simulation), gold triangles show "warmer–wetter" (PCM A2 scenario, 2071–2100, BCM simulation). Although the PCM A2 model projects unprecedented amounts of precipitation during winter months, it also projects lower water availability by April compared to current conditions. The GFDL A2 model projects significantly less water available in both the early and late months of the wet season compared to current conditions.

characterized by more significant inland valleys, a set which shows less than 0.25 °C separation among each other during the historical period, and displays a trend towards becoming even more convergent by the century's close. Values for precipitation display the spatial variability between basins, and significant differences between the PCM and GFDL model, in terms of estimated rainfall by the century's close: for the 2071–2100 time-period, the GFDL A2 scenario precipitation estimates range from 619 mm $y^{-1}$ for the Petaluma River basin to 790 mm $y^{-1}$ for the Marin Coast; under the PCM A2 scenario, precipitation ranges from 836 mm $y^{-1}$ for the Petaluma River basin to 1,023 mm $y^{-1}$ for the Marin Coast.

Plots of estimated runoff recharge (Figure 14A-H) reflect varying amounts of projected precipitation between scenarios and over time, but also show the effect of specific major basin characteristics. Particularly given climate change projections, the capacity of deep alluvium deposits in basins with significant valley formations provide the opportunity for significant recharge gains (at the expense of runoff), especially in Napa and Sonoma, under

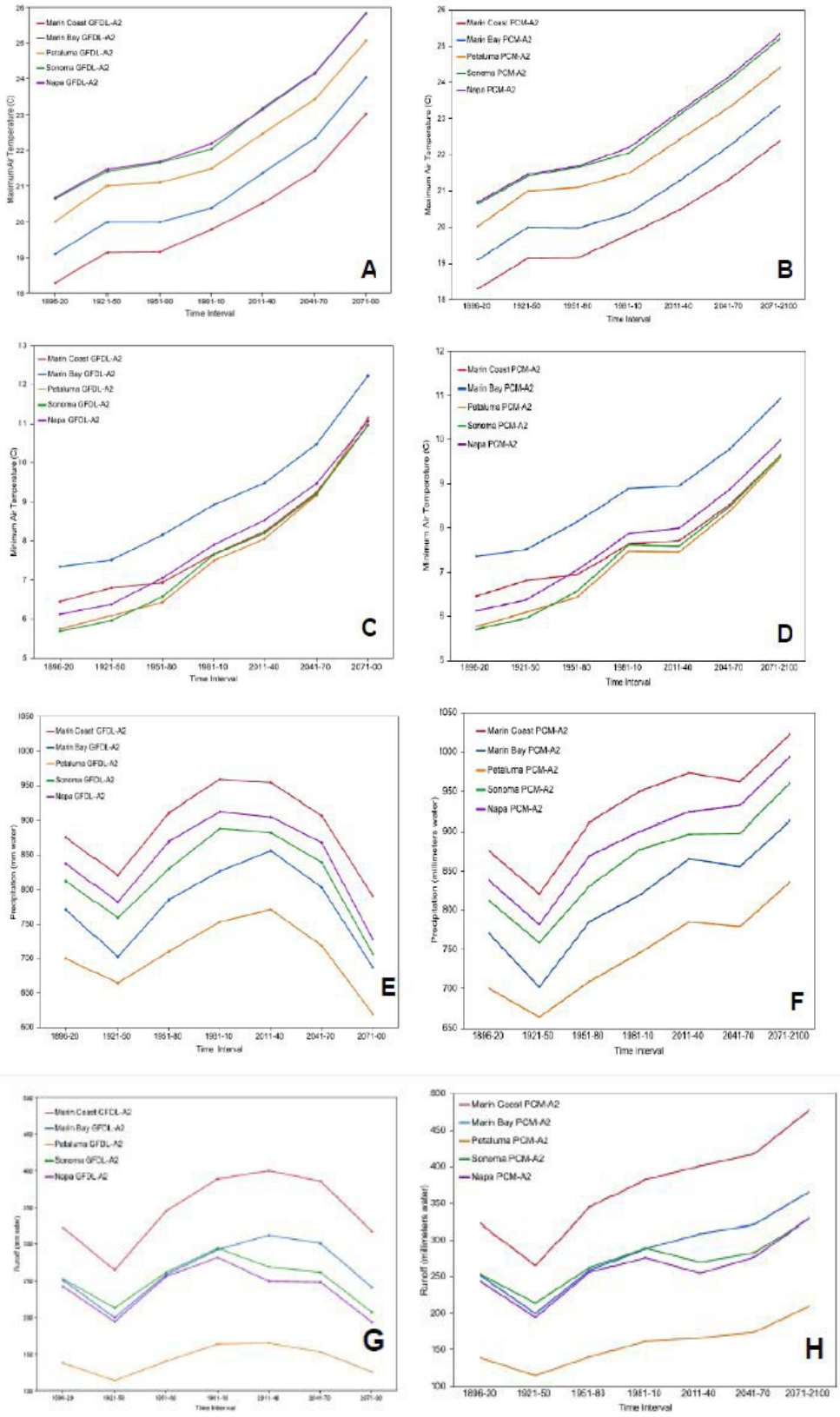


**Figures 14A–H** Historic (1896-2009) and projected (2010–2100) hydrology by major basin, North Bay region, GFDL-A2 and PCM-A2 scenarios. Plots compare major basin attributes for runoff, recharge, potential evapotranspiration, and water deficit for GFDL A2 and PCM A2 scenarios for major planning basins of study area. See Appendix B for results shown in a table.

high-precipitation scenarios (Figure 14D). Lacking subsurface storage capacity, the Marin Coast and Bay basins show a tendency towards converting increased precipitation directly to runoff (Figure 14C-D).

Under both scenarios, regardless of variations in precipitation, PET and CWD are projected to climb steadily through time for all basins (Figure 14E-H). CWD shows a steeper rate of change than PET for the GFDL A2 scenario (Figure 14G). Higher quantities of excess rainfall mitigate this effect for the PCM A2 scenario (Figure 14H). Napa and Sonoma, with the largest areas of inland valleys prone to warming, display on the order of 50 mm $y^{-1}$ greater CWD than the Marin Coast (Figure 14G–H).

## CONCLUSIONS

- The North Bay has already experienced a significant warming trend over the last century, with monthly maximum temperatures having increased approximately 1.4 ± 0.5 °C between 1901 and 2000.
- The spatial distribution of climate change to date is variable, with a trend towards warming of valley bottoms and, in some cases, cooling of montane areas. Coastal influences in general mitigate the warming trend, such that effects are more pronounced with increasing distance from the Pacific Coast or the Bay.
- The two climate models analyzed in this study represent the implications of future precipitation remaining comparable to today's precipitation versus a wetter future (approximately 20% more precipitation) in the context of a warmer climate.
- There is more uncertainty in projected precipitation trends than in projected temperature trends. Historic patterns of precipitation are highly variable, and, given the effects of temperature forcing on coupled climate–hydrologic processes, temporal and spatial variability of precipitation, runoff, recharge, and stream discharge is likely to increase.
- Hydrologic models predict reduced early and late wet-season runoff for the next century, resulting in a potentially extended dry season, for both wetter and drier future climate scenarios. Scenarios that estimate increased precipitation project that precipitation to be concentrated in mid-winter months, a trend which could increase the risk of floods.
- Evapotranspiration and associated climatic water deficit is projected to increase steadily in both the wetter and drier future scenarios, with values for the 2071–2100 period projected to be 5% to 20% higher than the 1981–2010 period, which translates to approximately 40 to 150 mm additional water needed on average to maintain current soil moisture conditions. Summers are projected to be longer and drier in the future than in the past regardless of precipitation trends.

### Management Applications

- While general circulation models converge on consistent temperature projections for the region given a range of emissions scenarios, they do not provide consistent projections about future precipitation. The discrepancy between the models is from assumptions about long-term climate cycles over the Pacific Ocean, and the relative arbitrariness of assigning a particular time value to start or end such a cycle in the process of modeling. Thus, it is important for watershed managers to consider a range of future precipitation scenarios and effects on runoff, recharge, and climatic water deficit. Arguably, the higher the projected rate of climate change for a subbasin, the more vulnerable resources may be in terms of the adaptation challenge. Our results point to some general results that may apply well beyond our case study area. Methods demonstrated here provide managers with the ability to query future climate–hydrology scenarios down to the scale of sub-basins to assess potential effects to a specific watershed, reservoir, or flood management zone. In arid climates, while water supply may be subject to increased

variability (e.g., reduced reliability) because of higher variability in precipitation, water demand is likely to steadily increase because of increased rates of evapotranspiration and climatic water deficit during extended summers.

- Extended dry season conditions and the potential for extended drought combined with unprecedented precipitation events may serve as additional stressors on water quality and habitat.
- It is worth noting, according to Cayan and others (2008), that a 10% to 20% change in annual precipitation is not a minor gain or loss. In the historical record, a 15% reduction in precipitation is sufficient to cast a year into the lowest third of the annual totals, and, since runoff is a non-linear outcome of precipitation, lessening the supply can in many cases drive runoff disproportionately lower.
- Recharge rates may prove less sensitive to variability in precipitation than runoff. The effect of variable precipitation on rates of recharge appear dampened during dry periods and exaggerated during wet periods. For example, in the drier GFDL A2 scenario for end-of-century, given an 11% reduction in precipitation, runoff declines by 13%, while recharge declines by only 2%. Conversely, for the PCM A2 model, given a 20% increase in precipitation, runoff is increased 20%, while recharge is up by 43%. This suggests that during dry years recharge will not suffer as large a reduction as runoff, while in wet years there will be a greater benefit in terms of recharge relative to runoff. These results point to the value of sound groundwater management, where applicable, as a critical climate adaptation strategy.
- By focusing on the relationship between soil moisture storage and evapotranspiration pressures, climatic water deficit integrates the effects of increasing temperature and variable precipitation on watershed conditions.
- Translating the climatic variability we anticipate over time into terms that people understand based on today's spatial variability may prove to be an effective communication approach. For example, translating a 2 °C difference in average maximum temperatures to the difference we experience today between the climates of the coast of Marin and Napa Valley, may prove to be a potent analogy to meaningfully convey the effect of climate change.
- Real-time monitoring of hydrological variables, as laid out in the NBWA Watershed Indicators report (Ridolfi and others 2010) and related efforts, will be central to testing the hypotheses about potential climate change demonstrated in this report, and to equip managers to respond to climate adaptation challenges in a timely fashion.

We conclude that for effective adaptive watershed management it will be critical to develop future scenarios using models capable of accurately representing historical regional climate and hydrology. Physically based watershed models and finely downscaled climate projections can effectively represent environmental processes at local watershed scales, and can be used to generate planning scenarios that incorporate climate effects on the water cycle. Our analysis shows under both higher and lower precipitation scenarios for an arid region, climatic water deficit is projected to increase no matter what, implying greater water demand if maintaining current land cover is a management objective. We demonstrate that assessing effects on the hydrologic cycle (rather than just on temperature and precipitation) will be central to effective water resource planning. Our results also show that by using empirical topography, soils, and geologic data at the finest spatial and temporal resolution available, scenarios can delineate significant differences between basins in terms of response to climate change. While managers should not rely on these projections for deterministic short-term weather predictions, downscaled watershed scenarios can be useful to define a range of potential conditions, and to identify long-term underlying trends that operate at the decadal to century scales common to all scenarios. Next steps in improving these downscaled products will entail the development of statistically meaningful estimates of

recurrence probabilities for extreme events currently outside the scope of monthly averages, including drought and floods that are contingent on finer temporal-scale hydrologic variations. However, given the current state-of-the-science, we recommend downscaling to the watershed scale as a starting point to identify potential long-term trends and to "bookend" ranges of physically possible scenarios.

## ACKNOWLEDGMENTS

The authors acknowledge the North Bay Watershed Association for core project funding, and U.S. Geological Survey, Bay Area Open Space Council, Pepperwood Foundation, Creekside Center for Earth Observation, and Switzer Foundation for supplemental support. We thank David Ackerly and the Gordon and Betty Moore Foundation's Terrestrial Biodiversity Climate Change Collaborative (TBC3) for helping us to expand applications of this work. We are also grateful to numerous colleagues who provided input on previous drafts of this study.

## REFERENCES

Bouwer LM, Aerts JC, Van de Coterlet GM, Van de Giesen N, Gieske A, Mannaerts C. 2004. Evaluating downscaling methods for preparing global circulation model (GCM) data for hydrological impact modeling. In: Aerts JC, Droogers P, editors. Climate change in contrasting river basins. London, UK: CAB International Publishing. p 25–47.

CalWater. 1999. California Interagency Watershed Map of 1999 (CalWater Version 2.2.1). Prepared by the Natural Resources Conservation Service California Interagency Watershed Mapping Committee. Available from: *http://cain.ice.ucdavis.edu/calwater/*.

Cayan DR, Maurer EP, Dettinger MD, Tyree M, Hayhoe K. 2008. Climate change scenarios for the California region. Climatic Change 87(Iss 1 Sppl):21–42. doi 10.1007/s10584–007–9377–6. Available from: *http://link.springer.com/article/10.1007%2Fs10584-007-9377-6*.

Cayan DR, Tyree M, Dettinger MD, Hidalgo H, Das T. 2009. California climate change scenarios and sea level rise estimates for the California 2008 Climate Change Scenarios Assessment. California Energy Commission Report No. CEC–500–2009–014–F. Available from: *http://www.energy.ca.gov/2009publications/CEC-500-2009-014/CEC-500-2009-014-F.pdf*.

Cornwell WK, Stuart S, Ramirez A, Dolanc CR, Thorne JH, Ackerly DD. 2012. Climate change impacts on California vegetation: physiology, life history, and ecosystem change. California Energy Commission. Publication number: CEC-500-2012-023. Available from: *http://www.energy.ca.gov/2012publications/CEC-500-2012-023/CEC-500-2012-023.pdf*.

Daly C, Gibson WP, Doggett M, Smith J, Taylor G. 2004. Up-to-date monthly climate maps for the conterminous United States. In: Proceedings of the 14th AMS Conference on Applied Climatology; 2004 Jan 13–16; Seattle. Seattle (WA): American Meteorological Society. 84th AMS Annual Meeting combined preprints. P5.1, CD-ROM. Available from: *http://www.prism.oregonstate.edu/pub/prism/docs/appclim04-uptodate_monthly_climate_maps-daly.pdf*.

Delworth TL and others. 2006. GFDL's CM2 global coupled climate models. Part 1. Formulation and simulation characteristics. Journal of Climate 19:643–674.

Flint LE, Flint AL. 2007. Regional analysis of groundwater recharge. In: Stonestrom DA, Constantz J, Ferré TPA, Leake SA, editors. Ground-water recharge in the arid and semiarid southwestern United States. Professional Paper 1703. Reston (VA): U.S. Geological Survey. Available from: *http://pubs.usgs.gov/pp/pp1703/b/*.

Flint LE, Flint AL. 2012a. Simulation of climate change in San Francisco Bay Basins, California: Case studies in the Russian River Valley and Santa Cruz Mountains. U.S. Geological Survey Scientific Investigations Report 2012–5132, 55 p. Available from: *http://pubs.usgs.gov/sir/2012/5132/*.

Flint LE, Flint AL. 2012b. Downscaling future climate scenarios to fine scales for ecological modeling and analysis. Ecological Processes 1:2. Available from: *http://www.ecologicalprocesses.com/content/1/1/2*.

Hidalgo H, Dettinger MD, Cayan DR. 2008. Downscaling with constructed analogues-daily precipitation and temperature fields over the United States. California Energy Commission Report No. CEC-500-2007-123. Available from: *http://meteora.ucsd.edu/cap/pdffiles/analog_pier_report.pdf*.

[IPCC] Intergovernmental Panel on Climate Change. 2001. Climate change 2001: the third assessment report (TAR) of the United Nations Intergovernmental Panel on Climate Change. Available from: *hhttp://www.grida.no/publications/other/ipcc_tar/*.

[IPCC] Intergovernmental Panel on Climate Change. 2007. Synthesis report. In: Pachauri RK, Reisinger A, editors. Climate Change 2007: the fourth assessment report (AR4) of the United Nations Intergovernmental Panel on Climate Change. Geneva, Switzerland: IPCC. 104 p. Available from: *http://www.ipcc.ch/publications_and_data/ar4/syr/en/contents.html*.

Knowles N, Cayan D. 2002. Potential effects of global warming on the Sacramento–San Joaquin watershed and the San Francisco Estuary. Geophysical Research Letters 29(18):1891. doi:10.1029/2001GL014339. Available from: *http://sfbay.wr.usgs.gov/publications/pdf/knowles_2002_global_warming.pdf*.

Loarie SR, Duffy PB, Hamilton H, Asner GP, Field CB, Ackerly DD. 2009. The velocity of climate change. Nature 462:72–76.

Meehl GA, Washington WM, Wigley TML, Arblaster JM, Dai A. 2003. Solar and greenhouse gas forcing and climate response in the twentieth century. Journal of Climate 16(3):426–444.

Nakic´enovic´ N, Alcamo J, Davis G, de Vries B, Fenhann J, Gaffin S, Gregory K, Grubler A, Jung TY, Kram T. 2000. Intergovernmental panel on climate change special report on emissions scenarios. Cambridge, UK: Cambridge University Press. Available from: *http://www.grida.no/publications/other/ipcc_sr/?src=/climate/ipcc/emission/index.htm*.

Nalder IA, Wein RW. 1998. Spatial interpolation of climatic normals: test of a new methods in the Canadian boreal forest. Agricultural and Forest Meteorology 92:211–225.

[NBWA] North Bay Watershed Association. 2003. North Bay watershed stewardship plan. Novato (CA): North Bay Watershed Association. 61 p.

[NRCS] Natural Resources Conservation Service. 2006. U.S. general soil map (STATSGO2). Available from: *http://soils.usda.gov/survey/geography/statsgo/description.html*.

Ridolfi K, Vorster P, Micheli L. 2010. Indicators and performance measures for North Bay watersheds. Prepared for the North Bay Watershed Association. Alameda (CA): San Francisco Estuary Institute. 36 p.

Stephenson NL. 1998. Actual evapotranspiration and deficit: biologically meaningful correlates of vegetation distribution across spatial scales: Journal of Biogeography 25(5):855–870.

Stouffer RJ and others. 2006. GFDL's CM2 global coupled climate models. Part 4. Idealized climate response. Journal of Climate 19:723–740.

Washington WM, Weatherly JW, Meehl GA, Semtner AJ, Bettge TW, Craig AP, Strand WG, Arblaster J, Wayland VB, James R, Zhang Y. 2000. Parallel climate model (PCM) control and transient simulations. Climate Dynamics 16:755–774.

[BAOSC] Bay Area Open Space Council. 2011. The conservation lands network: San Francisco Bay area upland habitat goals project report. Berkeley (CA): Bay Area Open Space Council. 306 p. Available from: *http://openspacecouncil.org/link/FullReport*.

# APPENDIX A: MAJOR AND MINOR BASIN DESCRIPTORS DERIVED FROM CALWATER, 1999

## *Marin Coast Major Basin*

| Model | Time interval | $T_{max}$ | | $T_{min}$ | | PPT | | Runoff | | Recharge | | PET | | CWD | |
|---|---|---|---|---|---|---|---|---|---|---|---|---|---|---|---|
| | | °C | SE | °C | SE | mm $y^{-1}$ | SE | mm $y^{-1}$ | SE | mm $y^{-1}$ | SE | mm $y^{-1}$ | SE | mm $y^{-1}$ | SE |
| Historic[a] | 1896-20 | 18.3 | 0.1 | 6.5 | 0.1 | 876 | 258 | 323 | 43 | 88 | 7 | 1122 | 2 | 655 | 12 |
| | 1921-50 | 19.1 | 0.1 | 6.8 | 0.1 | 820 | 260 | 265 | 33 | 86 | 7 | 1129 | 4 | 657 | 14 |
| | 1951-80 | 19.2 | 0.1 | 6.9 | 0.1 | 911 | 296 | 346 | 41 | 96 | 8 | 1129 | 4 | 658 | 13 |
| | 1981-10 | 19.8 | 0.1 | 7.7 | 0.1 | 960 | 357 | 383 | 49 | 92 | 8 | 1160 | 4 | 684 | 14 |
| GFDL A2[b] | 2011-40 | 20.5 | 0.1 | 8.2 | 0.1 | 955 | 72 | 400 | 54 | 77 | 8 | 1175 | 2 | 696 | 15 |
| | 2041-70 | 21.4 | 0.1 | 9.2 | 0.1 | 907 | 62 | 387 | 52 | 72 | 6 | 1197 | 3 | 746 | 11 |
| | 2071-00 | 23.0 | 0.1 | 11.0 | 0.1 | 790 | 72 | 318 | 54 | 58 | 7 | 1236 | 3 | 818 | 18 |
| GFDL B1[b] | 2011-40 | 20.5 | 0.1 | 8.3 | 0.1 | 998 | 91 | 474 | 72 | 75 | 8 | 1172 | 2 | 722 | 12 |
| | 2041-70 | 21.1 | 0.1 | 8.9 | 0.1 | 952 | 59 | 396 | 48 | 78 | 6 | 1188 | 2 | 710 | 11 |
| | 2071-00 | 21.6 | 0.1 | 9.3 | 0.1 | 790 | 56 | 287 | 43 | 57 | 7 | 1197 | 2 | 748 | 11 |
| PCM A2[b] | 2011-40 | 20.5 | 0.1 | 7.7 | 0.1 | 974 | 71 | 401 | 56 | 79 | 8 | 1166 | 2 | 671 | 14 |
| | 2041-70 | 21.3 | 0.1 | 8.5 | 0.1 | 963 | 65 | 418 | 54 | 74 | 7 | 1186 | 2 | 713 | 11 |
| | 2071-00 | 22.4 | 0.1 | 9.6 | 0.1 | 1023 | 88 | 477 | 72 | 73 | 7 | 1210 | 2 | 737 | 14 |
| PCM B1[b] | 2011-40 | 20.5 | 0.1 | 7.7 | 0.1 | 1156 | 86 | 586 | 69 | 89 | 8 | 1164 | 2 | 684 | 15 |
| | 2041-70 | 20.9 | 0.1 | 8.0 | 0.1 | 1025 | 82 | 463 | 70 | 74 | 7 | 1174 | 2 | 685 | 14 |
| | 2071-00 | 21.5 | 0.1 | 8.5 | 0.1 | 999 | 67 | 446 | 57 | 72 | 7 | 1186 | 2 | 703 | 13 |

a Derived from PRISM climate data (Daly and others 2004) and Basin Characterization Model (BCM) watershed simulations for historic time steps.
b Derived from referenced General Circulation Models climate projections and Basin Characterization Model (BCM) watershed simulations.

## *Marin Bay Major Basin*

| Model | Time interval | $T_{max}$ | | $T_{min}$ | | PPT | | Runoff | | Recharge | | PET | | CWD | |
|---|---|---|---|---|---|---|---|---|---|---|---|---|---|---|---|
| | | °C | SE | °C | SE | mm $y^{-1}$ | SE | mm $y^{-1}$ | SE | mm $y^{-1}$ | SE | mm $y^{-1}$ | SE | mm $y^{-1}$ | SE |
| Historic[a] | 1896-20 | 19.1 | 0.1 | 7.3 | 0.1 | 771 | 46 | 251 | 32 | 76 | 34 | 1,146 | 2 | 672 | 12 |
| | 1921-50 | 20.0 | 0.1 | 7.5 | 0.1 | 702 | 42 | 200 | 24 | 67 | 33 | 1,148 | 3 | 681 | 14 |
| | 1951-80 | 20.0 | 0.1 | 8.2 | 0.1 | 786 | 48 | 259 | 30 | 80 | 40 | 1,157 | 4 | 682 | 14 |
| | 1981-10 | 20.4 | 0.1 | 8.9 | 0.1 | 818 | 61 | 289 | 36 | 81 | 49 | 1,184 | 3 | 707 | 17 |
| GFDL A2[b] | 2011-40 | 21.4 | 0.1 | 9.5 | 0.1 | 856 | 68 | 313 | 41 | 80 | 11 | 1,203 | 10 | 713 | 17 |
| | 2041-70 | 22.3 | 0.1 | 10.5 | 0.1 | 803 | 56 | 301 | 38 | 72 | 8 | 1,226 | 14 | 765 | 12 |
| | 2071-00 | 24.0 | 0.1 | 12.2 | 0.1 | 687 | 64 | 242 | 40 | 58 | 8 | 1,267 | 16 | 839 | 18 |
| GFDL B1[b] | 2011-40 | 21.3 | 0.1 | 9.5 | 0.1 | 879 | 82 | 361 | 54 | 82 | 11 | 1,200 | 2 | 738 | 14 |
| | 2041-70 | 22.0 | 0.1 | 10.1 | 0.1 | 831 | 53 | 299 | 36 | 75 | 8 | 1,217 | 2 | 731 | 11 |
| | 2071-00 | 22.4 | 0.1 | 10.5 | 0.1 | 691 | 50 | 220 | 31 | 55 | 7 | 1,225 | 2 | 772 | 12 |
| PCM A2[b] | 2011-40 | 21.3 | 0.1 | 9.0 | 0.1 | 866 | 67 | 309 | 43 | 81 | 10 | 1,194 | 2 | 692 | 15 |
| | 2041-70 | 22.2 | 0.1 | 9.8 | 0.1 | 856 | 61 | 321 | 42 | 77 | 9 | 1,215 | 2 | 729 | 11 |
| | 2071-00 | 23.4 | 0.1 | 10.9 | 0.1 | 914 | 80 | 366 | 54 | 83 | 10 | 1,240 | 2 | 748 | 16 |
| PCM B1[b] | 2011-40 | 21.3 | 0.1 | 8.9 | 0.1 | 1,024 | 80 | 442 | 54 | 102 | 12 | 1,192 | 2 | 693 | 15 |
| | 2041-70 | 21.7 | 0.1 | 9.2 | 0.1 | 902 | 75 | 349 | 53 | 81 | 10 | 1,202 | 2 | 704 | 14 |
| | 2071-00 | 22.4 | 0.1 | 9.8 | 0.1 | 879 | 64 | 338 | 45 | 75 | 9 | 1,214 | 2 | 721 | 13 |

a Derived from PRISM climate data (Daly and others 2004) and Basin Characterization Model (BCM) watershed simulations for historic time steps.
b Derived from referenced General Circulation Models climate projections and Basin Characterization Model (BCM) watershed simulations.

## *Petaluma River Major Basin*

| Model | Time Interval | Tmax | | Tmin | | PPT | | Runoff | | Recharge | | PET | | CWD | |
|---|---|---|---|---|---|---|---|---|---|---|---|---|---|---|---|
| | | °C | SE | °C | SE | mm $y^{-1}$ | SE | mm $y^{-1}$ | SE | mm $y^{-1}$ | SE | mm $y^{-1}$ | SE | mm $y^{-1}$ | SE |
| Historic[a] | 1896-20 | 20.0 | 0.1 | 5.8 | 0.1 | 700 | 42 | 138 | 21 | 72 | 8 | 1155 | 2 | 663 | 18 |
| | 1921-50 | 21.0 | 0.1 | 6.1 | 0.1 | 664 | 39 | 115 | 15 | 66 | 7 | 1161 | 4 | 680 | 19 |
| | 1951-80 | 21.1 | 0.1 | 6.4 | 0.1 | 710 | 42 | 140 | 17 | 77 | 8 | 1166 | 4 | 676 | 19 |
| | 1981-10 | 21.5 | 0.1 | 7.5 | 0.1 | 745 | 54 | 162 | 23 | 80 | 11 | 1201 | 4 | 698 | 23 |
| GFDL A2[b] | 2011-40 | 22.5 | 0.1 | 8.1 | 0.1 | 771 | 58 | 166 | 23 | 94 | 14 | 1218 | 2 | 708 | 24 |
| | 2041-70 | 23.4 | 0.1 | 9.2 | 0.1 | 719 | 49 | 153 | 23 | 82 | 12 | 1242 | 3 | 760 | 17 |
| | 2071-00 | 25.1 | 0.1 | 11.2 | 0.2 | 619 | 58 | 126 | 23 | 66 | 12 | 1284 | 3 | 857 | 26 |
| GFDL B1[b] | 2011-40 | 22.5 | 0.1 | 8.1 | 0.2 | 805 | 73 | 208 | 34 | 108 | 99 | 1216 | 3 | 728 | 23 |
| | 2041-70 | 23.1 | 0.1 | 8.8 | 0.1 | 769 | 49 | 167 | 23 | 90 | 63 | 1233 | 2 | 721 | 18 |
| | 2071-00 | 23.6 | 0.1 | 9.3 | 0.1 | 649 | 46 | 124 | 20 | 64 | 50 | 1243 | 2 | 783 | 19 |
| PCM A2[b] | 2011-40 | 22.4 | 0.1 | 7.5 | 0.1 | 785 | 58 | 166 | 25 | 91 | 13 | 1209 | 2 | 682 | 22 |
| | 2041-70 | 23.3 | 0.1 | 8.4 | 0.1 | 779 | 51 | 174 | 24 | 91 | 13 | 1230 | 2 | 717 | 18 |
| | 2071-00 | 24.4 | 0.1 | 9.6 | 0.1 | 836 | 72 | 209 | 36 | 104 | 17 | 1256 | 2 | 734 | 25 |
| PCM B1[b] | 2011-40 | 22.5 | 0.1 | 0.1 | 0.2 | 805 | 73 | 208 | 34 | 108 | 18 | 1216 | 3 | 728 | 23 |
| | 2041-70 | 23.1 | 0.1 | 0.1 | 0.1 | 769 | 49 | 167 | 23 | 90 | 11 | 1233 | 2 | 721 | 18 |
| | 2071-00 | 23.6 | 0.1 | 0.1 | 0.1 | 649 | 46 | 124 | 20 | 64 | 9 | 1243 | 2 | 783 | 19 |

a Derived from PRISM climate data (Daly and others 2004) and Basin Characterization Model (BCM) watershed simulations for historic time steps.
b Derived from referenced General Circulation Models climate projections and Basin Characterization Model (BCM) watershed simulations.

## *Sonoma Creek Major Basin*

| Model | Time Interval | Tmax | | Tmin | | PPT | | Runoff | | Recharge | | PET | | CWD | |
|---|---|---|---|---|---|---|---|---|---|---|---|---|---|---|---|
| | | °C | SE | °C | SE | mm $y^{-1}$ | SE | mm $y^{-1}$ | SE | mm $y^{-1}$ | SE | mm $y^{-1}$ | SE | mm $y^{-1}$ | SE |
| Historic[a] | 1896-20 | 20.7 | 0.1 | 5.7 | 0.1 | 812 | 48 | 253 | 31 | 84 | 7 | 1,173 | 2 | 697 | 16 |
| | 1921-50 | 21.4 | 0.1 | 6.0 | 0.1 | 759 | 44 | 214 | 23 | 81 | 6 | 1,173 | 4 | 713 | 18 |
| | 1951-80 | 21.7 | 0.1 | 6.6 | 0.1 | 830 | 48 | 262 | 26 | 90 | 8 | 1,186 | 4 | 710 | 18 |
| | 1981-10 | 22.0 | 0.1 | 7.7 | 0.1 | 876 | 62 | 289 | 33 | 94 | 10 | 1,220 | 4 | 727 | 23 |
| GFDL A2[b] | 2011-40 | 23.2 | 0.1 | 8.2 | 0.1 | 883 | 66 | 269 | 33 | 118 | 15 | 1,240 | 13 | 746 | 22 |
| | 2041-70 | 24.2 | 0.1 | 9.2 | 0.1 | 840 | 57 | 262 | 34 | 107 | 12 | 1,263 | 15 | 792 | 17 |
| | 2071-00 | 25.9 | 0.1 | 11.0 | 0.2 | 706 | 65 | 207 | 32 | 85 | 12 | 1,301 | 17 | 886 | 24 |
| GFDL B1[b] | 2011-40 | 23.1 | 0.1 | 8.4 | 0.1 | 931 | 86 | 325 | 49 | 130 | 18 | 1,240 | 3 | 764 | 20 |
| | 2041-70 | 23.8 | 0.1 | 9.1 | 0.1 | 875 | 57 | 261 | 32 | 114 | 12 | 1,255 | 2 | 756 | 16 |
| | 2071-00 | 24.3 | 0.1 | 9.5 | 0.1 | 747 | 53 | 209 | 29 | 84 | 10 | 1,265 | 2 | 810 | 18 |
| PCM A2[b] | 2011-40 | 22.1 | 0.1 | 7.6 | 0.1 | 878 | 62 | 289 | 33 | 95 | 10 | 1,219 | 4 | 726 | 22 |
| | 2041-70 | 23.6 | 0.1 | 8.0 | 0.1 | 897 | 45 | 276 | 26 | 116 | 9 | 1,241 | 2 | 736 | 13 |
| | 2071-00 | 25.2 | 0.1 | 9.6 | 0.1 | 961 | 84 | 329 | 50 | 128 | 17 | 1,277 | 2 | 773 | 22 |
| PCM B1[b] | 2011-40 | 23.1 | 0.1 | 7.6 | 0.1 | 1,073 | 78 | 389 | 44 | 156 | 18 | 1,229 | 2 | 701 | 20 |
| | 2041-70 | 23.6 | 0.1 | 7.9 | 0.1 | 931 | 79 | 300 | 47 | 121 | 16 | 1,238 | 2 | 728 | 22 |
| | 2071-00 | 24.3 | 0.1 | 8.5 | 0.1 | 923 | 65 | 297 | 39 | 116 | 12 | 1,252 | 2 | 742 | 19 |

a Derived from PRISM climate data (Daly and others 2004) and Basin Characterization Model (BCM) watershed simulations for historic time steps.
b Derived from referenced General Circulation Models climate projections and Basin Characterization Model (BCM) watershed simulations.

## *Napa River Major Basin*

| Model | Time interval | $T_{max}$ | | $T_{min}$ | | PPT | | Runoff | | Recharge | | PET | | CWD | |
|---|---|---|---|---|---|---|---|---|---|---|---|---|---|---|---|
| | | °C | SE | °C | SE | mm $y^{-1}$ | SE | mm $y^{-1}$ | SE | mm $y^{-1}$ | SE | mm $y^{-1}$ | SE | mm $y^{-1}$ | SE |
| Historic[a] | 1896-20 | 20.7 | 0.1 | 6.1 | 0.1 | 837 | 51 | 243 | 34 | 109 | 9 | 1178 | 2 | 691 | 15 |
| | 1921-50 | 21.5 | 0.2 | 6.4 | 0.1 | 782 | 46 | 195 | 25 | 104 | 9 | 1181 | 4 | 702 | 17 |
| | 1951-80 | 21.7 | 0.1 | 7.1 | 0.1 | 870 | 50 | 257 | 29 | 120 | 11 | 1194 | 4 | 702 | 16 |
| | 1981-10 | 22.2 | 0.1 | 7.9 | 0.1 | 913 | 61 | 282 | 35 | 123 | 12 | 1224 | 4 | 715 | 20 |
| GFDL A2[b] | 2011-40 | 23.2 | 0.1 | 8.5 | 0.1 | 905 | 70 | 250 | 36 | 153 | 19 | 1242 | 3 | 739 | 20 |
| | 2041-70 | 24.2 | 0.1 | 9.5 | 0.1 | 868 | 61 | 249 | 37 | 142 | 14 | 1264 | 3 | 785 | 16 |
| | 2071-00 | 25.8 | 0.1 | 11.1 | 0.1 | 728 | 67 | 194 | 35 | 109 | 15 | 1300 | 3 | 873 | 23 |
| GFDL B1[b] | 2011-40 | 23.2 | 0.1 | 8.4 | 0.1 | 967 | 90 | 323 | 54 | 164 | 21 | 1239 | 3 | 758 | 18 |
| | 2041-70 | 23.9 | 0.1 | 9.1 | 0.1 | 901 | 59 | 246 | 35 | 151 | 15 | 1254 | 3 | 749 | 14 |
| | 2071-00 | 24.3 | 0.1 | 9.5 | 0.1 | 772 | 56 | 197 | 32 | 110 | 13 | 1264 | 2 | 796 | 16 |
| PCM A2[b] | 2011-40 | 23.2 | 0.1 | 8.0 | 0.1 | 925 | 72 | 254 | 40 | 153 | 18 | 1234 | 2 | 716 | 19 |
| | 2041-70 | 24.2 | 0.1 | 8.9 | 0.1 | 932 | 62 | 276 | 40 | 150 | 15 | 1256 | 2 | 749 | 14 |
| | 2071-00 | 25.3 | 0.1 | 10.0 | 0.1 | 994 | 88 | 331 | 55 | 160 | 19 | 1280 | 2 | 774 | 20 |
| PCM B1[b] | 2011-40 | 23.2 | 0.1 | 8.0 | 0.1 | 1106 | 81 | 382 | 49 | 194 | 19 | 1233 | 2 | 703 | 18 |
| | 2041-70 | 23.7 | 0.1 | 8.3 | 0.1 | 955 | 82 | 292 | 51 | 150 | 18 | 1242 | 2 | 728 | 20 |
| | 2071-00 | 24.4 | 0.1 | 8.9 | 0.1 | 965 | 71 | 297 | 44 | 153 | 16 | 1257 | 2 | 740 | 18 |

a Derived from PRISM climate data (Daly and others 2004) and Basin Characterization Model (BCM) watershed simulations for historic time steps.
b Derived from referenced General Circulation Models climate projections and Basin Characterization Model (BCM) watershed simulations.

# APPENDIX B: MAJOR BASIN ASSESSMENTS (TABULAR FORMAT)

## *Major Basins*

| Major basin name | Selected drainages included | Area ($km^2$) | Area (acres) |
|---|---|---|---|
| Marin Coast | Lagunitas and San Geronimo Creeks, Bolinas | 833.7 | 206,012 |
| Marin Bay | Miller and Corte Madera Creeks | 341.5 | 84,396 |
| Petaluma River | Stage Gulch Creek | 384.9 | 95,114 |
| Napa River | Conn, York, Milliken, Soda and other Creeks | 829.2 | 204,890 |
| Sonoma Creek | Bear, Calabazas, Carriger, and Nathanson Creeks | 431.4 | 106,593 |

## *Minor Basins*

| Minor basin ID (HRC) | Minor basin (CalWater CDFPWSNAME) | CalWater HANAME | Major basin | Area ($km^2$) | Area (acres) |
|---|---|---|---|---|---|
| 1 | Upper Napa River | Napa River | Napa River | 24.9 | 6,165 |
| 2 | Garnett Creek | Napa River | Napa River | 20.6 | 5,088 |
| 3 | Simmons Canyon | Napa River | Napa River | 34.6 | 8,560 |
| 4 | Ritchie Creek | Napa River | Napa River | 35.5 | 8,772 |
| 5 | Bell Canyon Reservoir | Napa River | Napa River | 27.6 | 6,830 |
| 6 | Conn Creek | Napa River | Napa River | 29.5 | 7,297 |
| 7 | Moore Creek | Napa River | Napa River | 19.5 | 4,819 |
| 8 | York Creek | Napa River | Napa River | 34.2 | 8,451 |
| 9 | Chiles Creek | Napa River | Napa River | 29.5 | 7,293 |
| 10 | Fir Canyon | Napa River | Napa River | 33.2 | 8,195 |
| 11 | Heath Canyon | Napa River | Napa River | 41.0 | 10,139 |
| 12 | Lake Hennessey | Napa River | Napa River | 23.3 | 5,761 |
| 14 | Rector Reservation | Napa River | Napa River | 37.7 | 9,325 |
| 15 | Bear Canyon | Napa River | Napa River | 37.9 | 9,371 |
| 18 | Upper Dry Creek | Napa River | Napa River | 24.7 | 6,101 |
| 19 | Milliken Reservoir | Napa River | Napa River | 50.3 | 12,439 |
| 20 | Soda Creek | Napa River | Napa River | 28.6 | 7,070 |
| 22 | Lower Dry Creek | Napa River | Napa River | 23.0 | 5,679 |
| 24 | Redwood Creek | Napa River | Napa River | 28.2 | 6,978 |
| 29 | Spencer Creek | Napa River | Napa River | 36.6 | 9,039 |
| 30 | undefined | Napa River | Napa River | 38.7 | 9,565 |
| 34 | Browns Valley Creek | Napa River | Napa River | 24.6 | 6,068 |
| 59 | Mouth of Napa River | Napa River | Napa River | 145.2 | 35,883 |
| 13 | Mouth of Napa River | Napa River | n/a (adjacent Napa River) | 174.6 | 43,146 |
| 16 | Bear Creek | Sonoma Creek | Sonoma Creek | 21.4 | 5,296 |
| 17 | Upper Sonoma Creek | Sonoma Creek | Sonoma Creek | 49.1 | 12,140 |
| 21 | Upper Calabazas | Sonoma Creek | Sonoma Creek | 46.8 | 11,571 |
| 23 | Lower Calabazas | Sonoma Creek | Sonoma Creek | 48.9 | 12,073 |
| 26 | Nathanson Creek | Sonoma Creek | Sonoma Creek | 37.2 | 9,183 |

| Minor basin ID (HRC) | Minor basin (CalWater CDFPWSNAME) | CalWater HANAME | Major basin | Area ($km^2$) | Area (acres) |
|---|---|---|---|---|---|
| 27 | Mouth of Sonoma Creek | Sonoma Creek | Sonoma Creek | 122.5 | 30,259 |
| 38 | Haraszthy Creek | Sonoma Creek | Sonoma Creek | 28.6 | 7,068 |
| 40 | Champlin Creek | Sonoma Creek | Sonoma Creek | 19.0 | 4,686 |
| 43 | undefined | Sonoma Creek | Sonoma Creek | 30.4 | 7,513 |
| 60 | Mouth of Sonoma Creek | Sonoma Creek | Sonoma Creek | 27.5 | 6,804 |
| 28 | Lynch Creek | Petaluma River | Petaluma River | 42.4 | 10,485 |
| 31 | undefined | Petaluma River | Petaluma River | 96.9 | 23,948 |
| 32 | Adobe Creek | Petaluma River | Petaluma River | 36.5 | 9,016 |
| 37 | undefined | Petaluma River | Petaluma River | 60.2 | 14,869 |
| 42 | Upper San Antonio Creek | Petaluma River | Petaluma River | 33.0 | 8,156 |
| 45 | Stage Gulch | Petaluma River | Petaluma River | 30.3 | 7,476 |
| 46 | Lower San Antonio Creek | Petaluma River | Petaluma River | 60.2 | 14,864 |
| 47 | undefined | Petaluma River | Petaluma River | 25.5 | 6,301 |
| 48 | Stafford Lake | Novato | Marin Bay | 126.0 | 31,128 |
| 51 | Miller Creek | Novato | Marin Bay | 30.9 | 7,626 |
| 53 | San Anselmo Creek | San Rafael | Marin Bay | 74.0 | 18,277 |
| 54 | San Rafael Creek | San Rafael | Marin Bay | 29.3 | 7,252 |
| 56 | Old Mill Creek | San Rafael | Marin Bay | 8.4 | 2,081 |
| 61 | Gallinas Creek | Novato | Marin Bay | 26.5 | 6,549 |
| 62 | Belvedere Lagoon | San Rafael | Marin Bay | 4.8 | 1,182 |
| 63 | Belvedere Lagoon | San Rafael | Marin Bay | 6.9 | 1,698 |
| 64 | Belvedere Lagoon | San Rafael | Marin Bay | 5.0 | 1,246 |
| 65 | Belvedere Lagoon | San Rafael | Marin Bay | 3.7 | 902 |
| 67 | Old Mill Creek | San Rafael | Marin Bay | 0.8 | 197 |
| 68 | Old Mill Creek | San Rafael | Marin Bay | 15.7 | 3,888 |
| 69 | Old Mill Creek | San Rafael | Marin Bay | 9.6 | 2,378 |
| 25 | Ebabias Creek | Estero Americano | Marin Coast | 50.2 | 12,393 |
| 35 | Upper Stemple | Estero San Antonio | Marin Coast | 65.5 | 16,187 |
| 36 | Lower Stemple | Estero San Antonio | Marin Coast | 69.1 | 17,072 |
| 39 | Keys Creek | Tomales Bay | Marin Coast | 181.2 | 44,785 |
| 44 | Nicks Cove | Tomales Bay | Marin Coast | 61.9 | 15,302 |
| 49 | Nicasio Reservoir | Tomales Bay | Marin Coast | 95.7 | 23,638 |
| 50 | Tomasini Canyon | Tomales Bay | Marin Coast | 138.7 | 34,273 |
| 52 | San Geronomo Creek | Tomales Bay | Marin Coast | 24.3 | 6,000 |
| 55 | Pine Gulch Creek | Bolinas | Marin Coast | 40.7 | 10,066 |
| 57 | Fern Creek | Bolinas | Marin Coast | 31.8 | 7,869 |
| 58 | Rodeo Lagoon | Bolinas | Marin Coast | 14.3 | 3,542 |
| 71 | Rodeo Lagoon | Bolinas | Marin Coast | 7.6 | 1,884 |
| 72 | Audubon Canyon | Bolinas | Marin Coast | 5.8 | 1,436 |
| 73 | Pine Gulch Creek | Bolinas | Marin Coast | 1.1 | 284 |

| Minor basin ID (HRC) | Minor basin (CalWater CDFPWSNAME) | CalWater HANAME | Major basin | Area ($km^2$) | Area (acres) |
|---|---|---|---|---|---|
| 76 | Laguna Lake | Tomales Bay | Marin Coast | 11.1 | 2,747 |
| 77 | Keys Creek | Tomales Bay | Marin Coast | 12.4 | 3,055 |
| 78 | Ebabias Creek | Estero Americano | Marin Coast | 23.6 | 5,824 |
| 73 | Tomales Bay | Keys Creek | n/a | 12.4 | 3,055 |
| 74 | Estero Americano | Ebabias Creek | n/a | 23.6 | 5,824 |
| 75 | Napa River | Upper Napa River | n/a | 24.9 | 6,165 |